Session 11

Spacecraft Center-of-Mass Modeling

Graham Appleby, Toshi Otsubo

CoM Implementation Issues

Van Husson, HTSI
ILRS CB

Background

- In Nov 1996, SLR CSTG accepts Husson and Sinclair's proposal for reporting system configuration changes via configuration files and NP indicators
- Never got 100% participation
- ILRS Site Logs contain the same information as the configuration files, but have no pointers (i.e. no indexes) to the NP Flags

Configuration and Detector Flags

- Multi-Detector Systems
  - Herstmonceux (interchange SPAD and CSPAD)
  - Zimmerwald (blue-CSPAD, IR- PMT)
  - Wettzell (APD for LAGEOS and HEO, MCP for LEO and LAGEOS)
  - McDonald (MCP for LEO and LAGEOS, PMT for HEO and Lunar)
  - TIGO at Concepcion (CSPAD, APD, PMT)
  - Matera (MCP and streak camera/MCP)
- Systems one with detector, but different threshold levels (HSLR and non-HSLR)
  - NASA MOBLAS (Yarragadee, Greenbelt, Haleakala, Hartebeesthoek, Monument Peak, Tahiti)

Configuration Reporting Problems

- Configuration files are not current or missing and flags are inverted and/or mis-understood
  - EUROLAS
    - Herstmonceux, Zimmerwald, Wettzell, Concepcion, San Fernando, Matera, Potsdam3, Grasse (LLR), FTLRS
  - NASA
    - No problems
  - WPLTN
    - Beijing, BeijingA, Changchun

Network Data Screening Levels

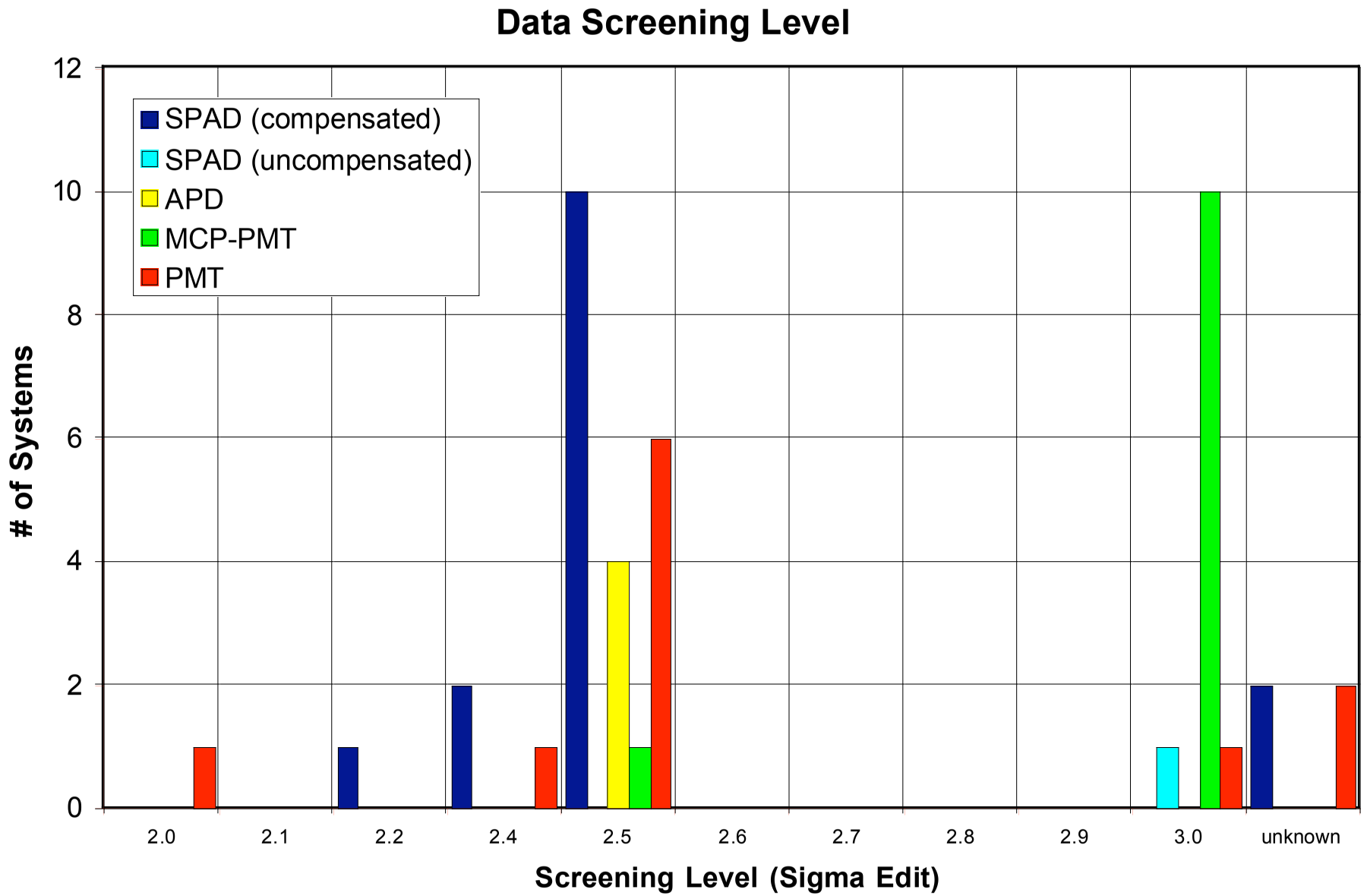

CoM Implementation Issues

- Proper use of system configuration indicators and the detector type in the NPs (header bytes 46 & 47, respectively).
- Variable data screening (e.g. 2.2, 2.5, 3.0, etc.) levels
- Need indicators for:
  - Signal Strength Indicator (SPAD and APD)
  - Discriminator Internal Cable Length (PMT systems)
  - Laser Polarization Type?
  - Laser Pulse-Width?

Strawman Recommendations

- The current names of header record bytes 46 and bytes 47 are very confusing
  - Byte 46: System Change Indicator – a flag to indicator major changes to the system.
  - Byte 47: System Configuration Indicator – a flag to indicator alternate modes of operation
- Recommend changing the names to:
  - Byte 46: System Configuration Indicator – a flag to indicate major changes to the system.
  - Byte 47: Detector Indicator – a flag to indicator the detector in use
- Bytes 44 (epoch time scale) and bytes 45 (system calibration method) have outgrown their real usefulness
  - Better use could be a indicator for data screening and discriminator cable length and/or laser polarization
  - For example, Byte 44:
    - 0 – 3.0 sigma edit
    - 1 – 2.5 sigma edit
    - 2 – 2.0 sigma edit

Strawman Recommendations

- NP data record bytes 48,49,50 are used for LLR, but not SLR (i.e. spare bytes)
- Currently the number of raw ranges compressed into the NP does not have enough bytes to support Khz lasers (bytes 44:47). Need at least 1 more byte.
- We need a flag to indicate average NP bin signal strength

Strawman Recommendations

- Standardize Detector Flags for the Network
  - For example, byte 47 is:
    - 1 – CSPAD (compensated channel)
    - 2 – SPAD (uncompensated channel)
    - 3 – MCP
    - 4 – PMT
    - 5 – APD
- Standardize the Screening Level for Each Detector Type (this would eliminate the need for a flag)
- Individual NPs contain Signal Strength info.
  - For example, in each NP reserve a byte for average energy level
    - 1 – single photon
    - 2 – few photons
    - 3 – 10 photons
    - 4 – 100 photons

Strawman Recommendations

- The Site Logs need pointers to the different configuration indicators contained in the normal points
- Data Formats and Procedures WG need to resolve these issues in close cooperation with the Networks and Engineering WG, the Signal Processing WG, and the Analysis WG

Engineering Verification of CoM Algorithms

- For a given SPAD station, take the full-rate and apply different screening levels and then compare the NPs from each set and note the difference in the NP OMCs.
- For systems with multi-detectors, take data in the same color simultaneously. Can this be done. It is like a 2-color experiment, except done in one color.

NATURAL ENVIRONMENT RESEARCH COUNCIL

CRL

Theoretical Centre-of-mass Corrections for LAGEOS, ETALON and AJISAI

See Otsubo and Appleby, JGR, 108, B4, 2201, Apr 200

Toshimichi OTSUBO

Communications Research Laboratory, Kashima, Japan

Graham M APPLEBY

Natural Environment Research Council, Monks Wood, UK

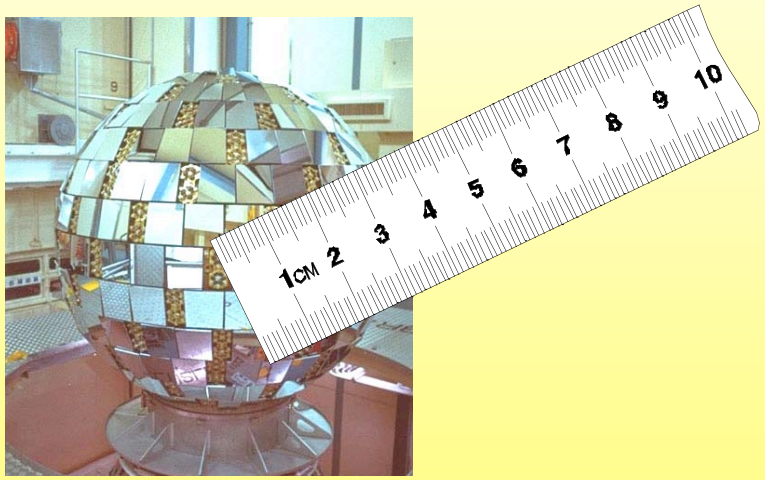

Laser Workshop 2003, Koetzting, 28-31 Oct 2003.

Satellite signature effect

- Multiple reflectors contributing to the satellite response.
- System-dependent detection timing
  - Single photon
  - C-SPAD
  - MCP-PMT

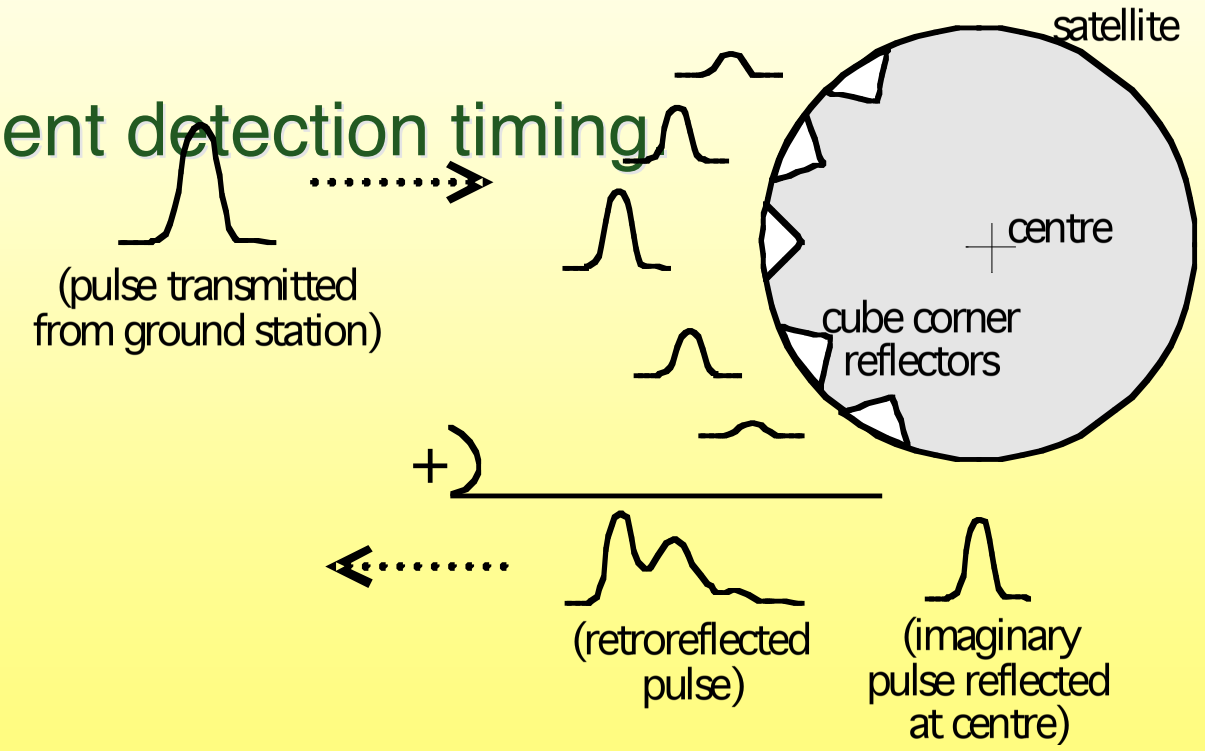

- Key error factor to achieve accurate GM and TRF

NATURAL ENVIRONMENT RESEARCH COUNCIL

CRL

LAGEOS(1&2)

US+Italy 1976, 92

Altitude 5900 km

Diameter 0.60 m

426 CCRs

AJISAI

Japan 1986

Altitude 1500 km

Diameter 2.15 m

1436 CCRs

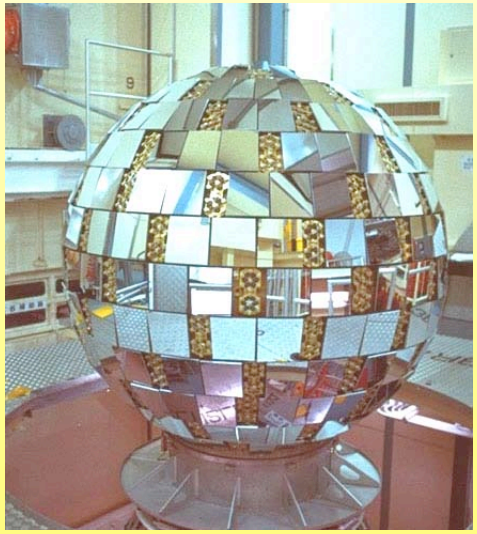

ETALON(1&2)

USSR 1989

Altitude 19000 km

Diameter 1.294 m

2134 CCRs

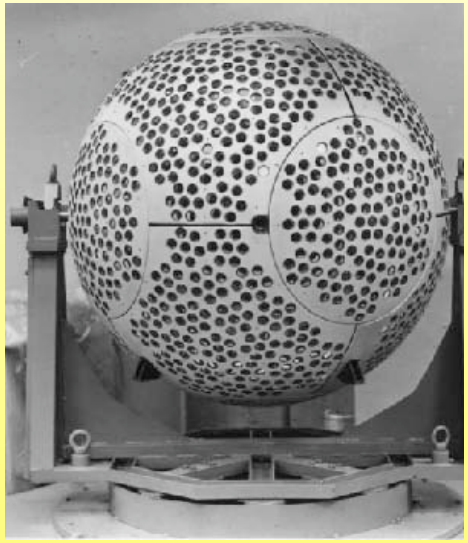

NATURAL ENVIRONMENT RESEARCH COUNCIL

CRL

Response from single reflector

- 3 factors to be considered.
  - –Effective reflection area (a)
  - –Reflectance (e)
  - –Diffraction
- How to compute the intensity.
  - $\propto ae$ … diffraction neglected.
  - $\propto a^2 e$ … simple diffraction model.

[Neubert, 1994; Otsubo, 1999]

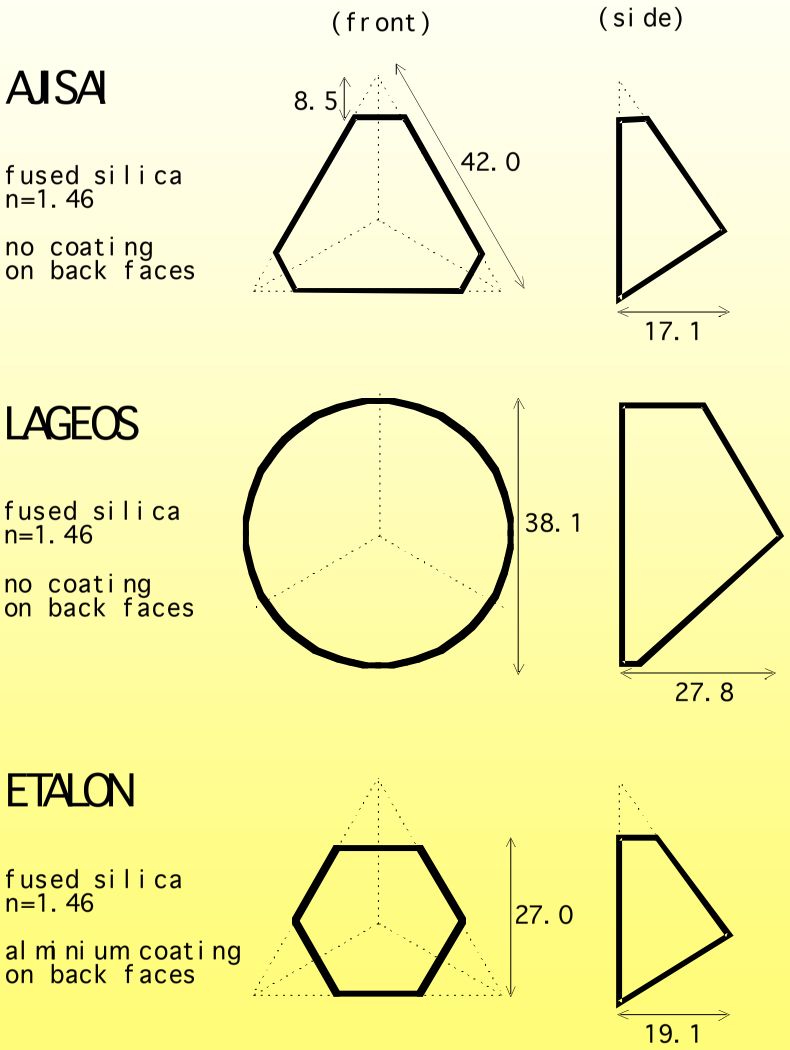

← Effective reflection area

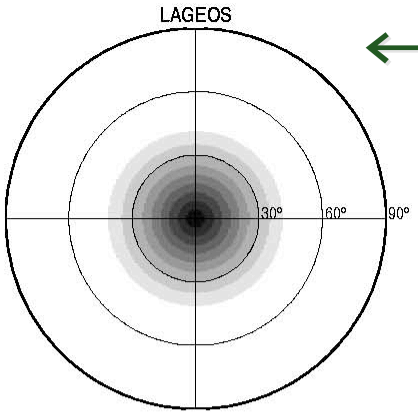

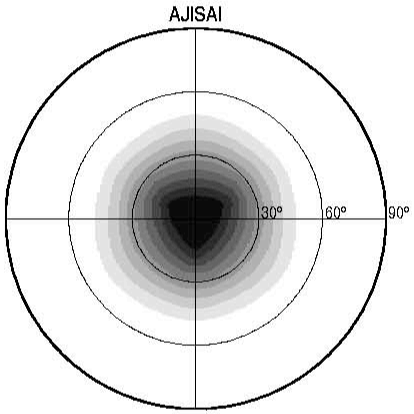

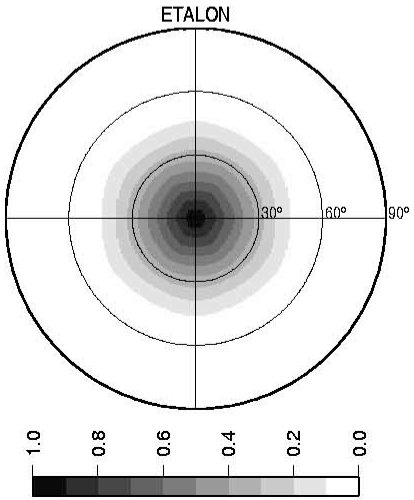

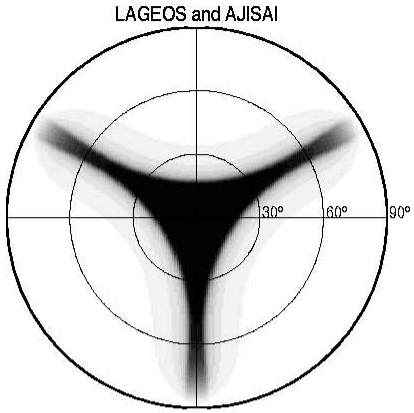

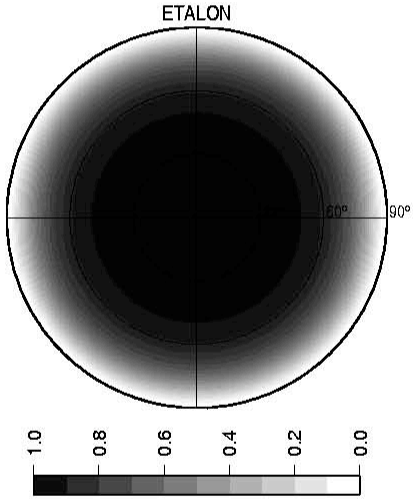

Reflectance

→

NATURAL ENVIRONMENT RESEARCH COUNCIL

Centre-of-mass correction

Extracted from Otsubo and Appleby, JGR, 108, B4, 2201, Apr

LAGEOS n=1.1

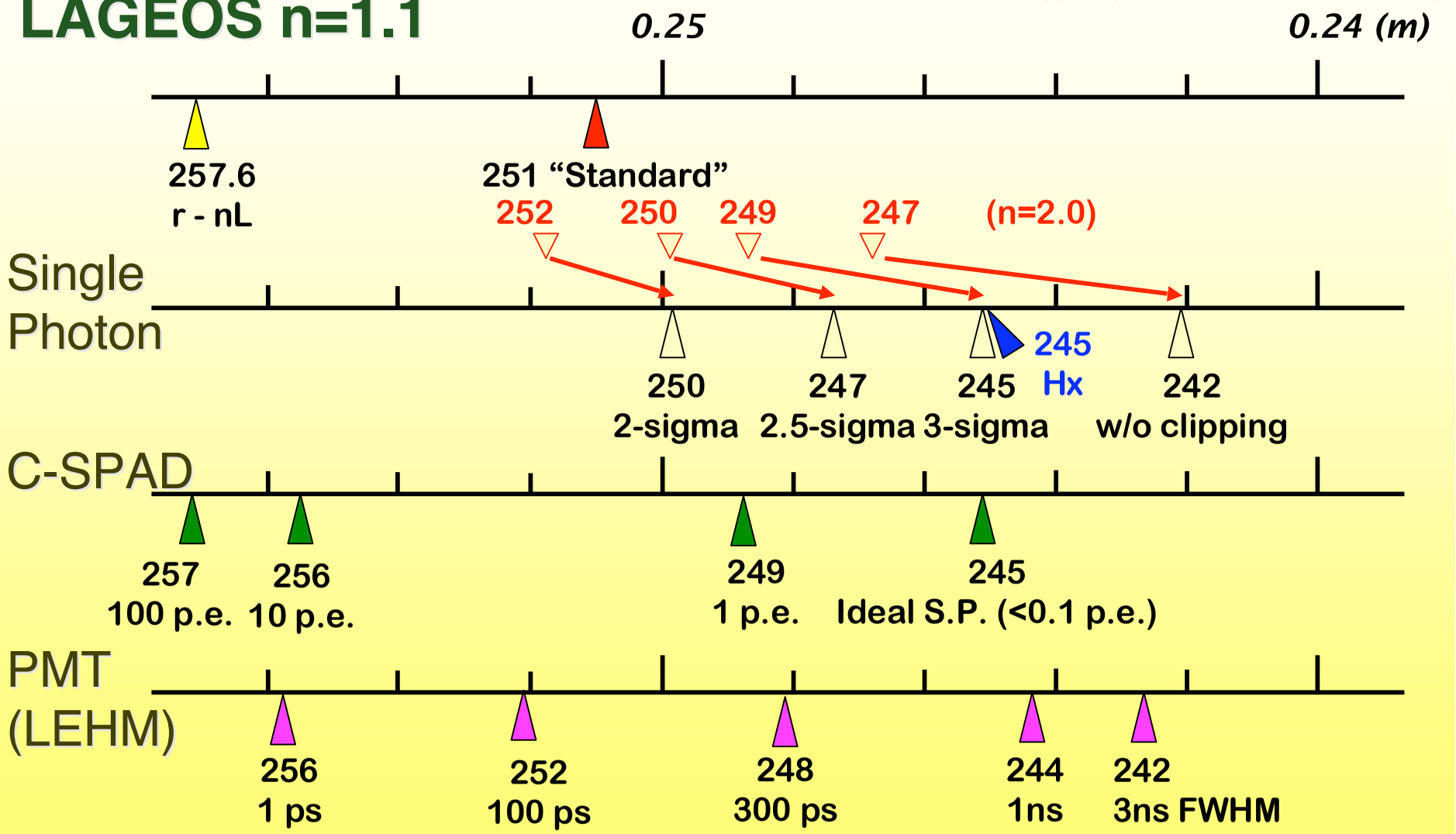

NATURAL ENVIRONMENT RESEARCH COUNCIL

Centre-of-mass correction

Extracted from Otsubo and Appleby, JGR, 108, B4, 2201, Apr

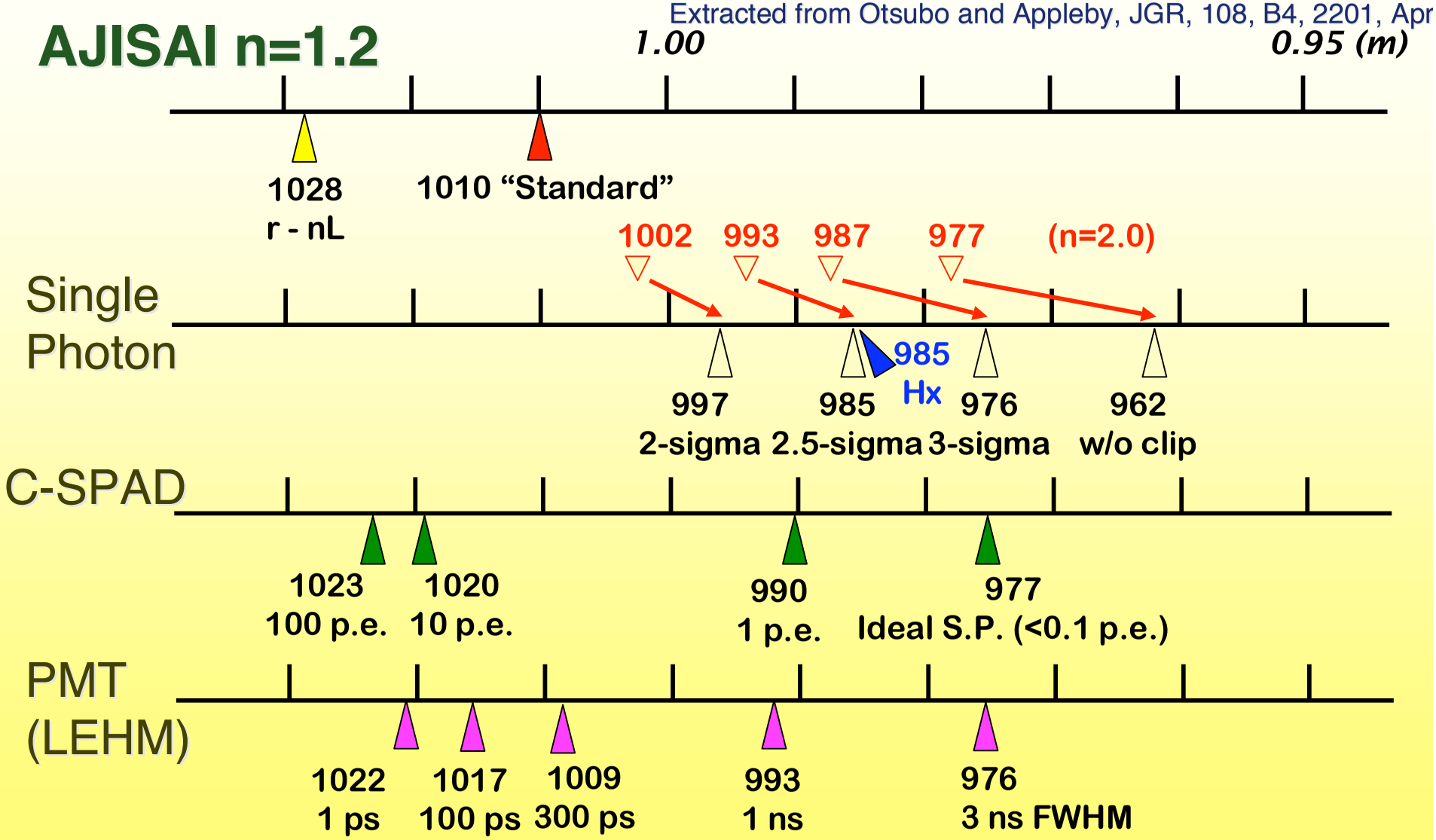

NATURAL ENVIRONMENT RESEARCH COUNCIL

Centre-of-mass correction

Extracted from Otsubo and Appleby, JGR, 108, B4, 2201, Apr

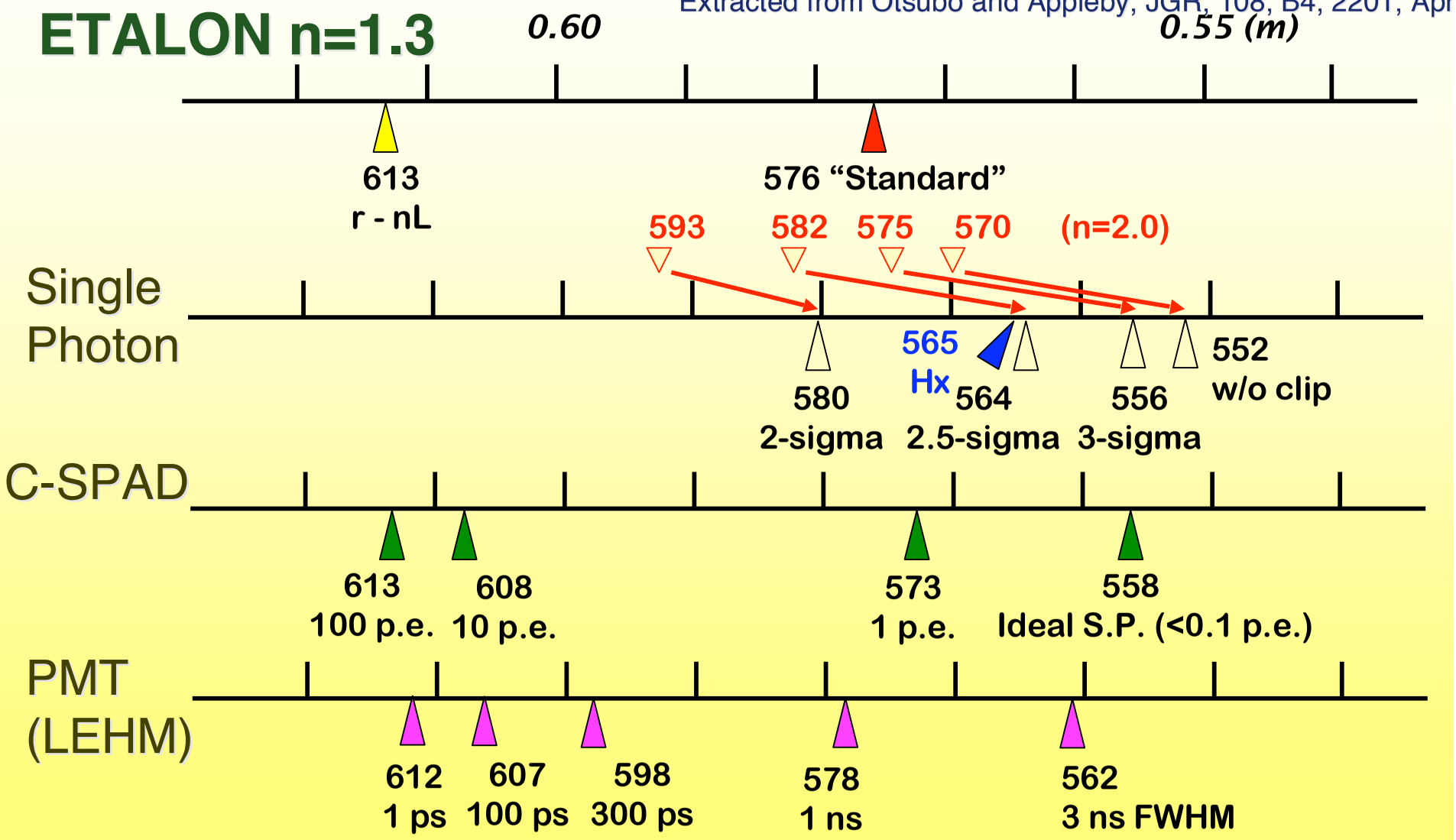

NATURAL ENVIRONMENT RESEARCH COUNCIL

CRL

Discussions (personal opinions) for mm ranging

- Avoid the intensity-dependent bias ON-SITE!
  - Likely to become the elevation-angle-dependent bias, which can significantly degrade the station height determination.
    - C-SPAD does NOT compensate the satellite returns. 1 cm for LAGEOS, 4-5 cm for AJISAI and ETALON.
    - MCP+CFD seems ok at 1-cm level, but not at 1-mm level.
  - Try the on-site shot-by-shot experiment.
  - kHz laser? Go for STRICT single photon!

Range residuals vs Intensity (Otsubo and Genba, DC Workshop, 2002)

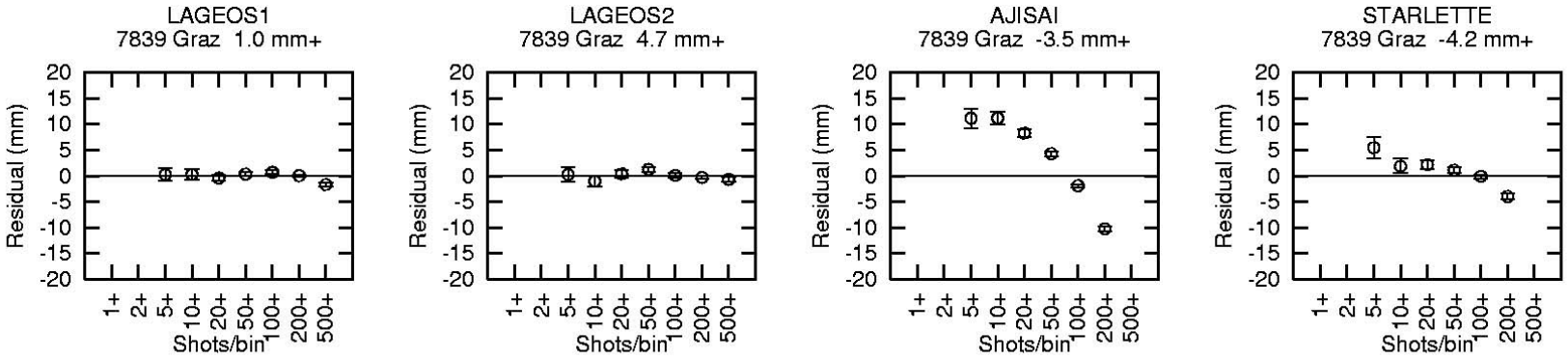

Range residuals vs Intensity (Otsubo and Genba, DC Workshop, 2002)

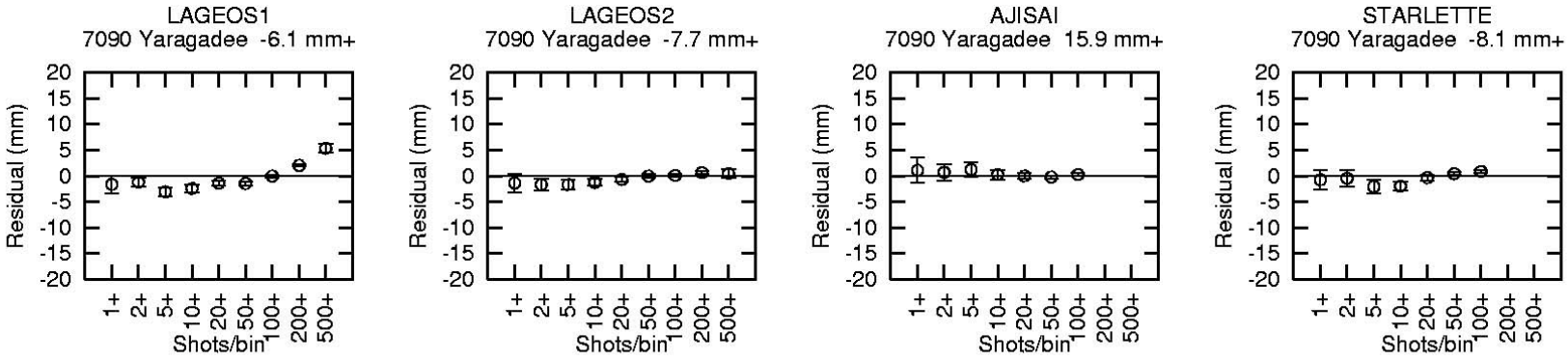

Range residuals vs Intensity (Otsubo and Genba, DC Workshop, 2002)

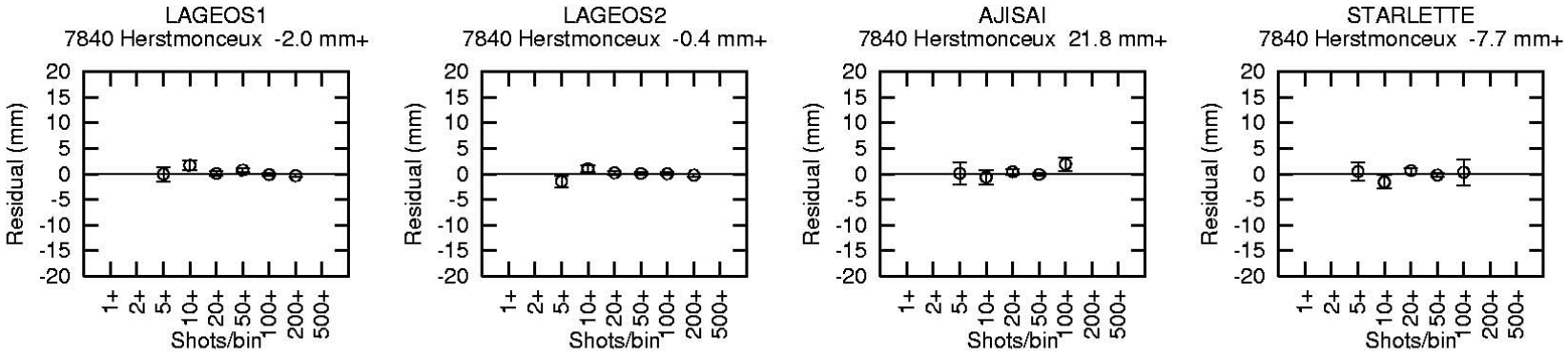

NATURAL ENVIRONMENT RESEARCH COUNCIL

CRL

Discussions (personal opinions) for mm analysis

- Better adjust the range bias for a while.
  - 1-mm accuracy is still a challenge.
    - Impossible to model the CoM correction for multi-photon (esp. MCP+CFD) systems at 1-mm accuracy.
    - Many other systematic error sources.
  - Accept a constant offset bias. Too risky to fix it to 0 mm.
  - Tight constraints can be applied if necessary.
  - A different story when all stations do the single photon.

NATURAL ENVIRONMENT RESEARCH COUNCIL

Summary

- Stations,
  - Eliminate any systematic range errors.
- Analysts,
  - Not assume zero range bias.
- English speakers,
  - Is the word “bias” appropriate? Probably negative impression to non-SLR people.

NATURAL ENVIRONMENT RESEARCH COUNCIL

CRL

Satellite Signature Effect in GLONASS SLR Data

Toshimichi OTSUBO

Communications Research Laboratory, Kashima, Japan

Graham M APPLEBY

Philip GIBBS

Natural Environment Research Council, Monks Wood, UK

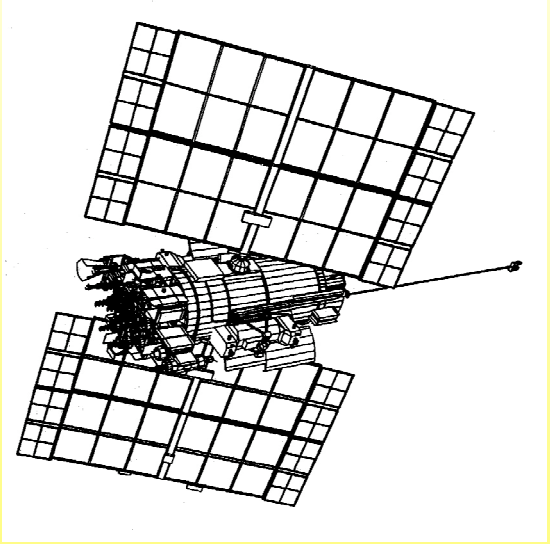

Laser Workshop 2003, Koetzting, 28-31 Oct 2003.

GLONASS CCR Array

Old type

- 396 CCRs.
- Until GLO-80.

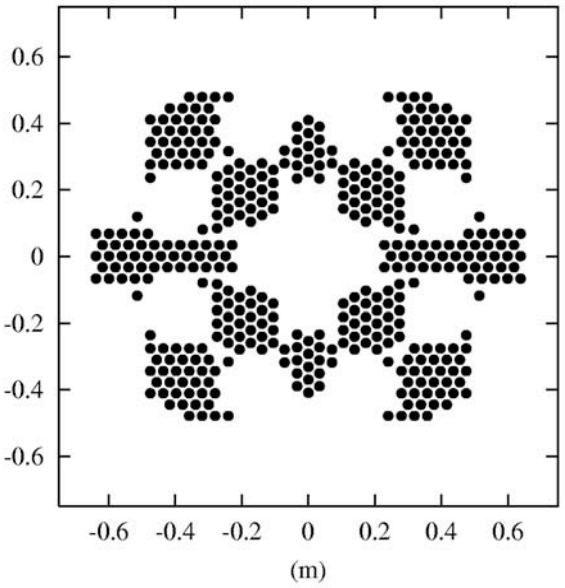

New type (except GLO-88)

- 132 CCRs.
- Since GLO-84.

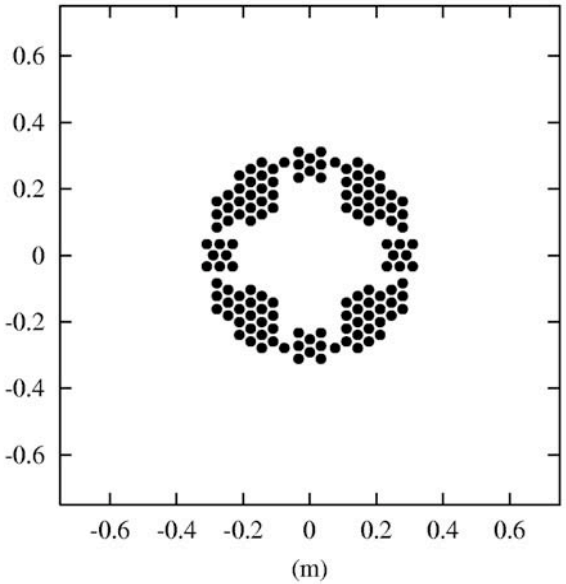

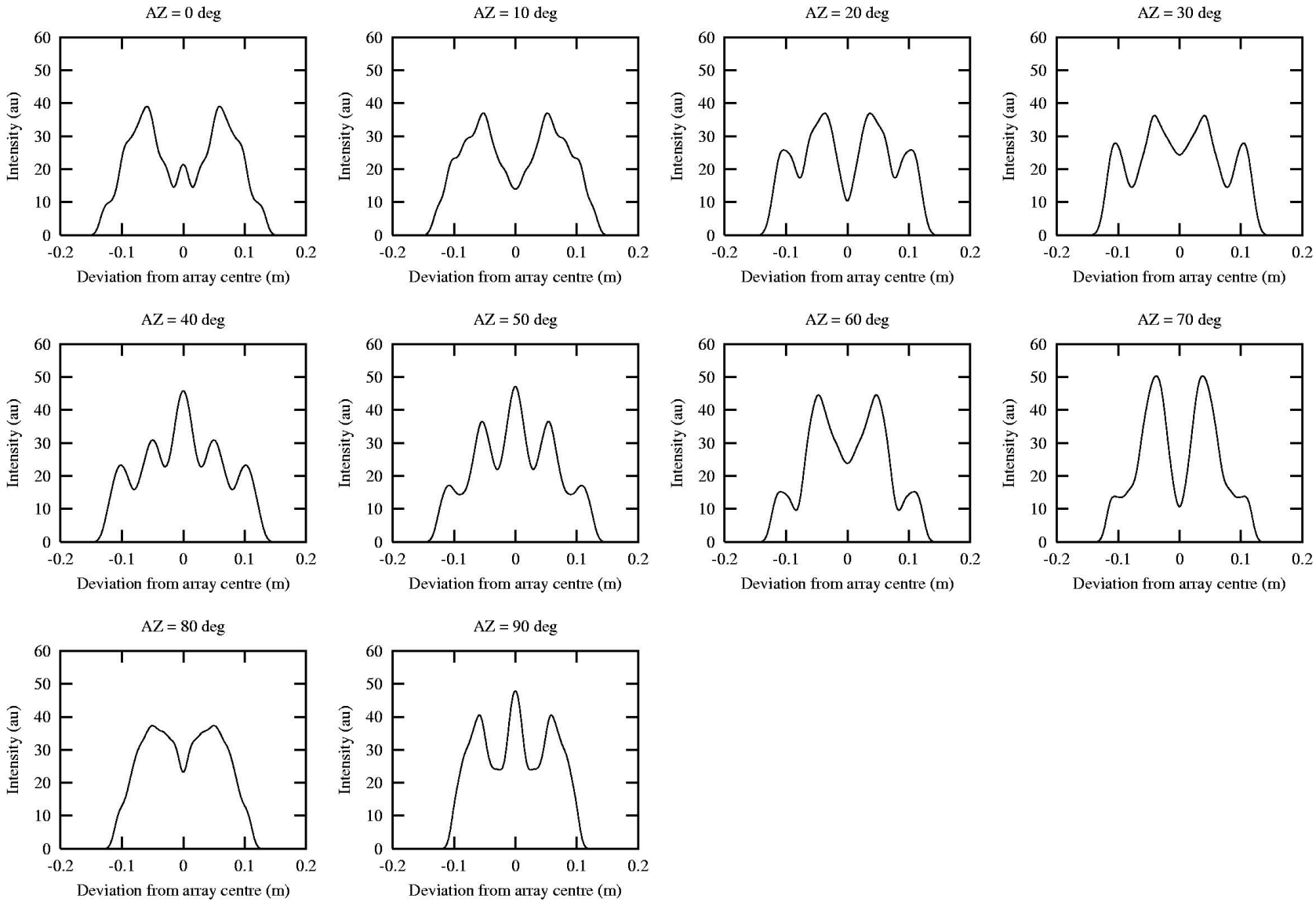
AZ = 0 deg
AZ = 10 deg
AZ = 20 deg
AZ = 30 deg
AZ = 40 deg
AZ = 50 deg
AZ = 60 deg
AZ = 70 deg
AZ = 80 deg
AZ = 90 deg
Intensity (au)
Deviation from array centre (m)
0
10
20
30
40
50
60
-0.2
-0.1
0
0.1
0.2

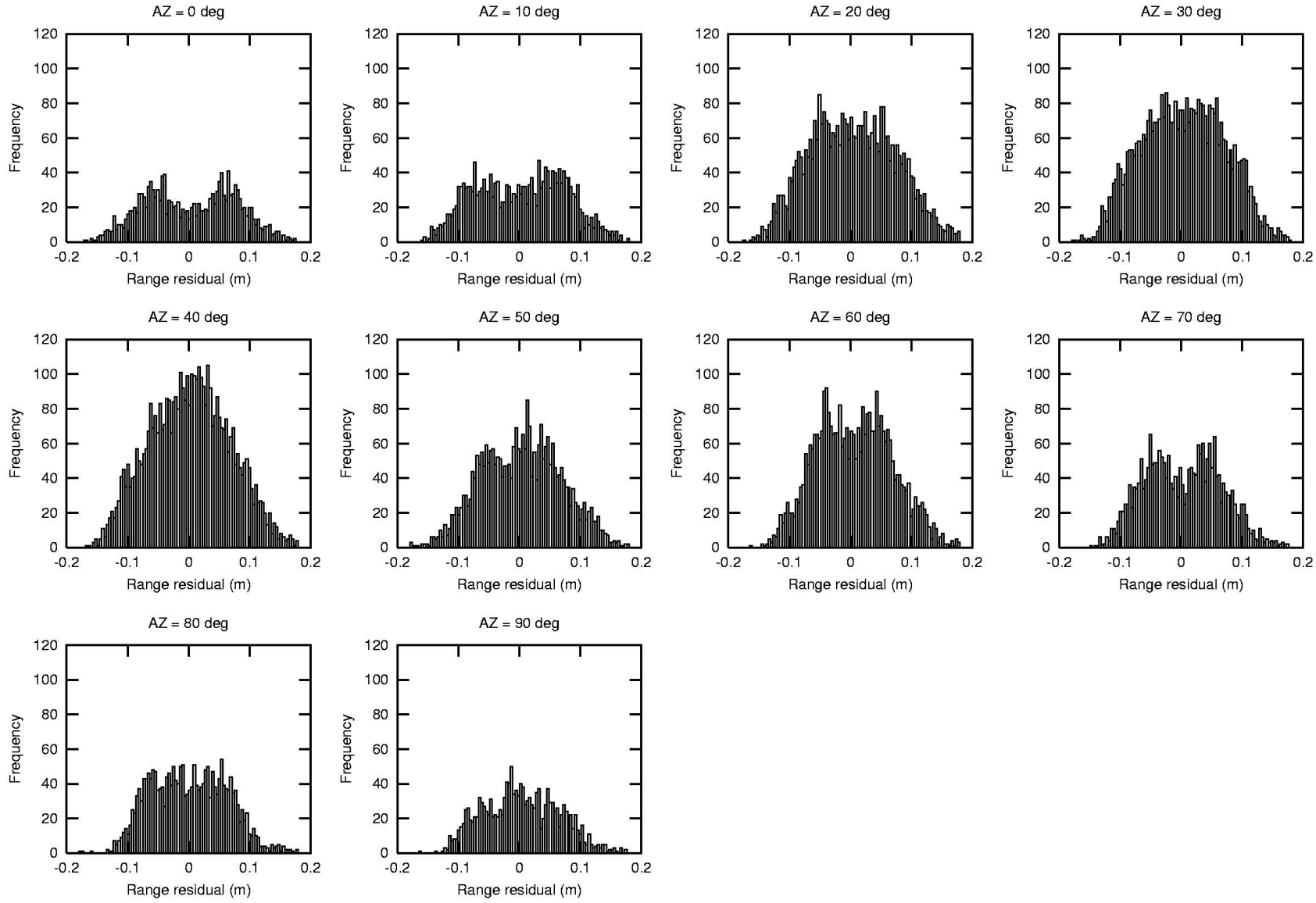
AZ = 0 deg
AZ = 10 deg
AZ = 20 deg
AZ = 30 deg
AZ = 40 deg
AZ = 50 deg
AZ = 60 deg
AZ = 70 deg
AZ = 80 deg
AZ = 90 deg
Frequency
Range residual (m)
0
20
40
60
80
100
120
-0.2
-0.1
0
0.1
0.2

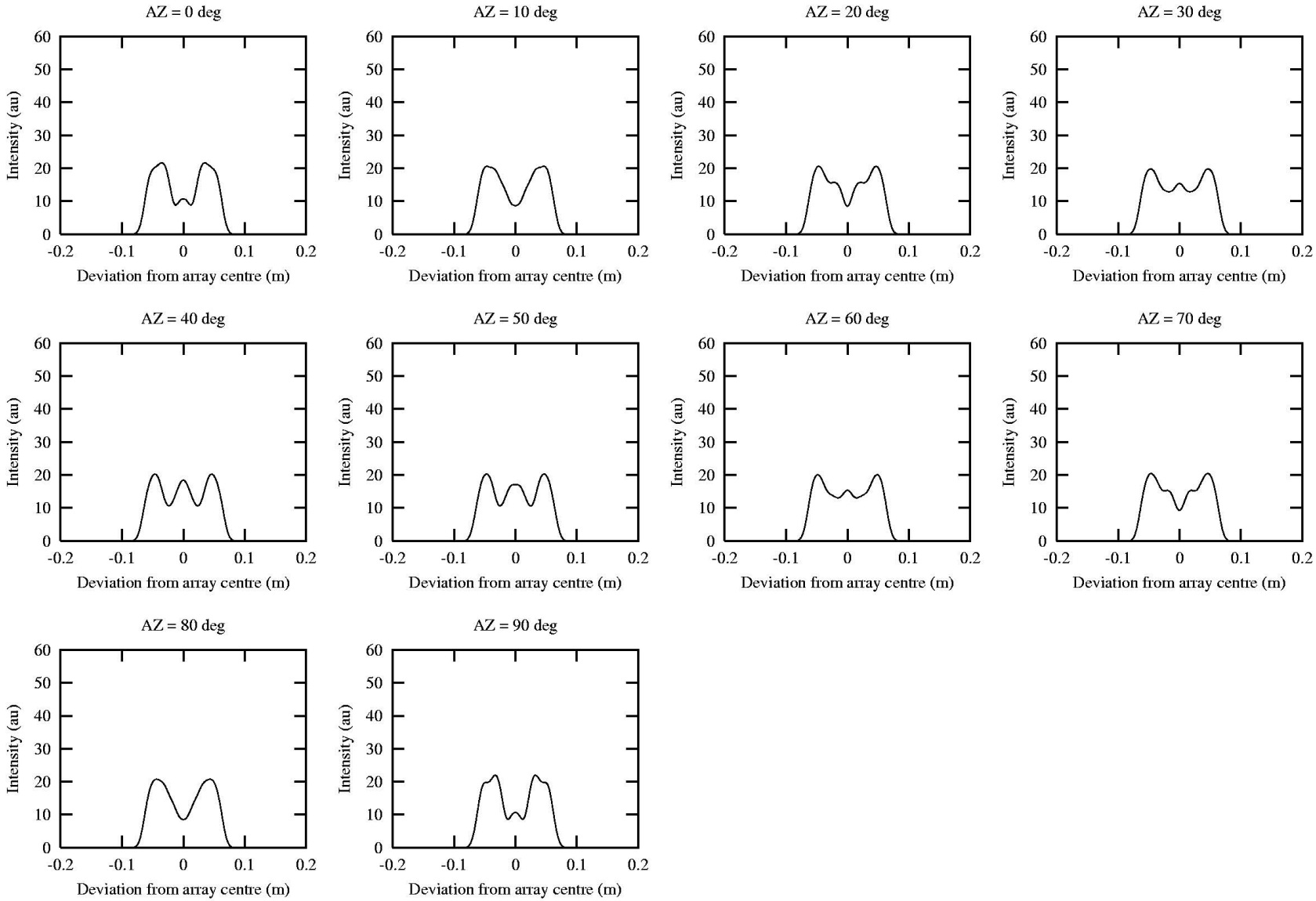
AZ = 0 deg
AZ = 10 deg
AZ = 20 deg
AZ = 30 deg
AZ = 40 deg
AZ = 50 deg
AZ = 60 deg
AZ = 70 deg
AZ = 80 deg
AZ = 90 deg
Intensity (au)
Deviation from array centre (m)
0
10
20
30
40
50
60
-0.2
-0.1
0
0.1
0.2

Effective array size estimation

- for 2001.
- estimated by concerto ver 3.
- bias

  elevation dependent

  average ～ (eff array size) x 0.15 .

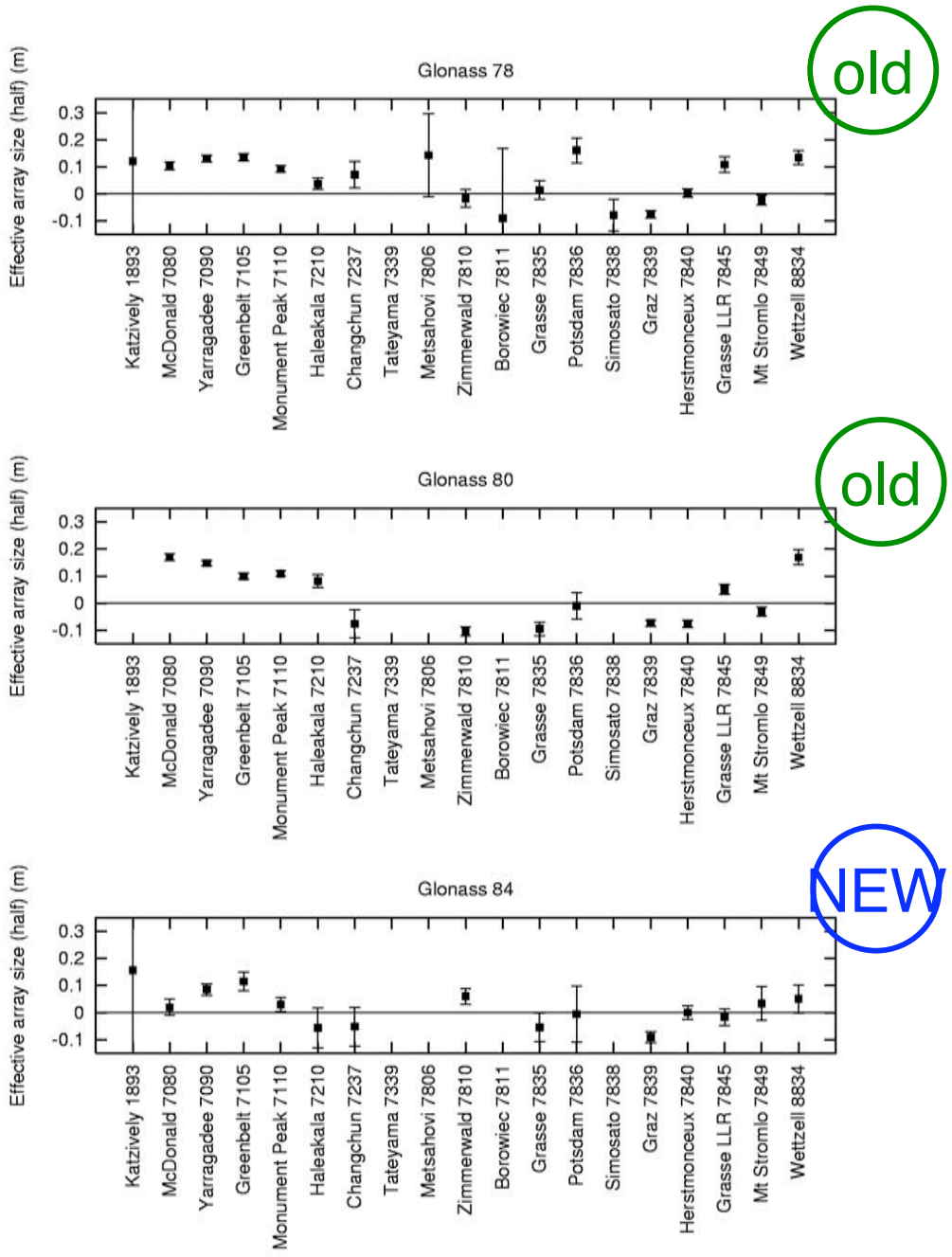

Effective array size estimation

- for 2002.

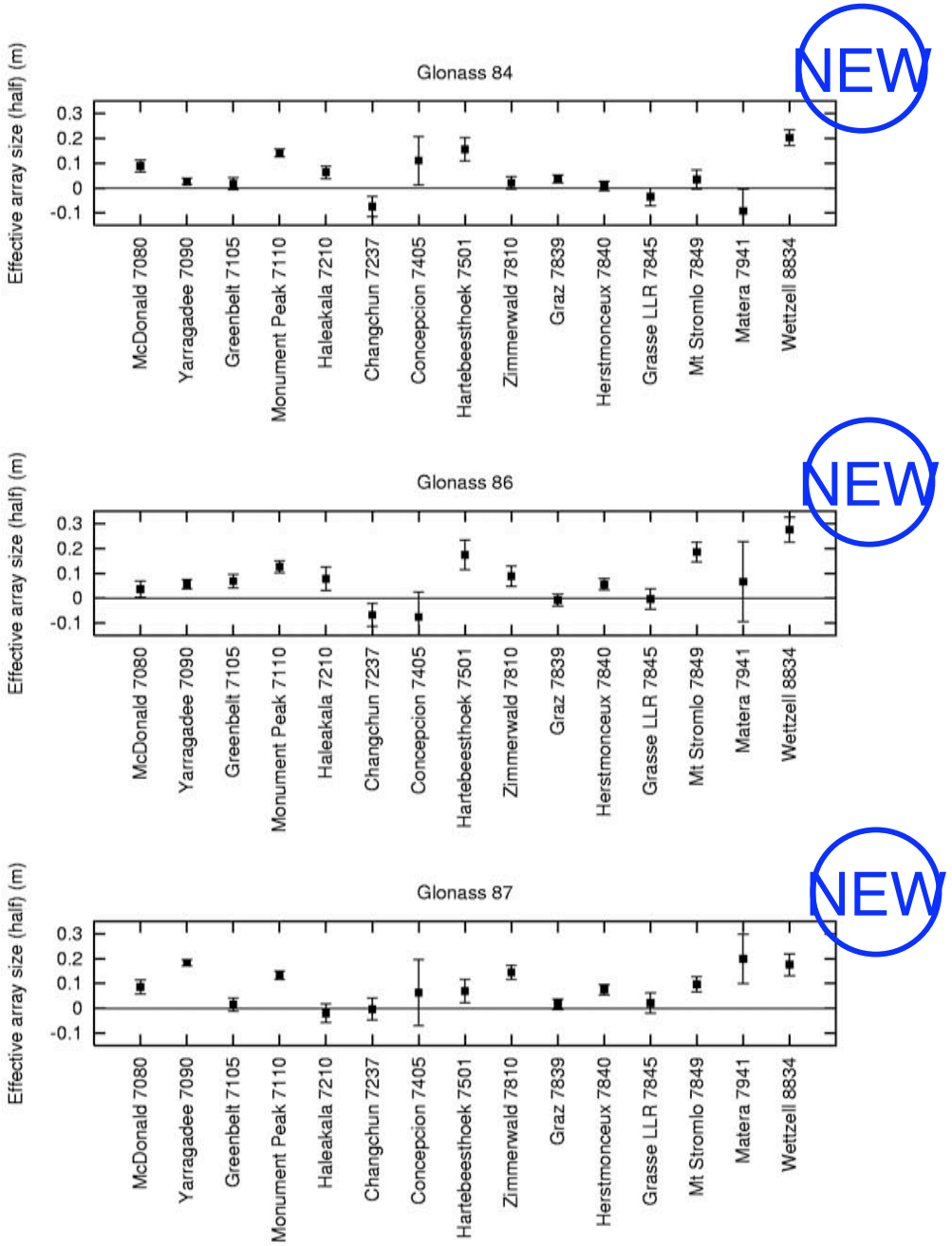

NATURAL ENVIRONMENT RESEARCH COUNCIL

CRL

Summary

- GLONASS CCR Design

  Large flat array is probably not the best idea. It causes the elevation-dependent range error. ~ 2 cm on average.

  New CCR array at least halved the signature effect. < 1 cm on ave.

- Return energy vs signature effect

  Difficult in observing new GLONASSes esp in daytime?

  What is the best array pattern for such high orbiters?

  How about in the GALILEO project?

CoM offset for ETALON 1 & 2 = ???

Erricos C. Pavlis
JCET/UMBC - NASA/Goddard/926

2003 ILRS Workshop
October 28 - 31, 2003, Kötzting, Germany

MM vs. MC

LAGEOS 1 & 2 Residual Statistics MM and MC Models

LAGEOS 1

Marini - Murray

	M-M Residual [m]
Minimum	-0.0537
Maximum	0.1872
Points	327
Mean	0.0504
Median	0.0402
RMS	0.0669
Std Deviation	0.0441

Mendes - Ciddor

	M-C Residual [m]
Minimum	-0.1266
Maximum	0.0965
Points	327
Mean	0.0280
Median	0.0276
RMS	0.0368
Std Deviation	0.0240

LAGEOS 2

	M-M Residual [m]
Minimum	-0.0666
Maximum	0.1607
Points	516
Mean	0.0345
Median	0.0333
RMS	0.0536
Std Deviation	0.0411

	M-C Residual [m]
Minimum	-0.1217
Maximum	0.1282
Points	516
Mean	0.0212
Median	0.0203
RMS	0.0442
Std Deviation	0.0388

A need for CoM offset for ETALON 1 & 2

- With an on-going campaign to intensively track the ETALON 1 & 2 spacecraft for Terrestrial Reference Frame improvement, the need for a credible CoM value valid for the variety of tracking systems surfaced in mid-2001
- After some "looking and asking around" we prompted an email response from Ron Noomen (June 2001)
- We initially adopted the values that were emailed by Ron Noomen, with the understanding that it was plausible that these values could and would change in the future, pending finalization of the responsible ILRS WG's results.

CoM offset for ETALON 1 & 2

- **CoM values adopted were emailed by Ron Noomen:**

From: Ron Noomen <Ron.Noomen@lr.tudelft.nl>
Subject: Etalon c.o.m.
To: ilrsac@cddisa.gsfc.nasa.gov (ILRS Analysis Centers),
ilrsaac@cddisa.gsfc.nasa.gov (ILRS Associate Analysis Centers),
ilrsawg@cddisa.gsfc.nasa.gov (ILRS Analysis Working Group)
Date: Thu, 14 Jun 2001 18:51:40 +0200 (MET)

…

Broadly:

- for strictly single-photon systems, use 560mm; e.g. Herstmonceux
- for CSPAD with higher-than-single photons, use 580mm; e.g. most of Europe;
- for MCP systems, use 610mm; e.g. the NASA systems.

Note:
The CoM value can vary by +/- 10mm according to (unknown) satellite orientation. Signal-strength variations are also potentially large.
Work to refine these values is ongoing.

…

Adopted CoM offset for ETALON 1 & 2 by site

- 18685901 -0.580

- 70802419 -0.610
- 70900513 -0.610
- 71050725 -0.610
- 71100411 -0.610
- 72102313 -0.610

- 72371901 -0.580
- 72496101 -0.580
- 73357201 -0.580
- 73397401 -0.580
- 73558401 -0.580

- 75010602 -0.610

- 78067601 -0.580
- 78106801 -0.580
- 78113802 -0.580
- 78208201 -0.580
- 78325501 -0.580
- 78353102 -0.580
- 78365801 -0.580
- 78372805 -0.580
- 78383602 -0.580
- 78393402 -0.580

- 78403501 -0.560

- 78457801 -0.580
- 78498001 -0.580
- 88341001 -0.580

- --other-- -0.580

E1 No Bias vs. ALL Adj. Bias

#Obs.	Mean	RMS	Site	# Obs.	Mean	RMS
252	0.0099	0.0186	MOBL7090	252	0.0000	0.0108
73	0.0000	0.0225	MTLR7501	73	0.0000	0.0148
41	0.0000	0.0137	WLRS8834	41	0.0000	0.0091
37	0.0158	0.0203	HALE7210	37	0.0000	0.0114
6	-0.0079	0.0248	MOBL7110	6	0.0000	0.0203
9	0.0227	0.0251	MLRS7080	9	0.0000	0.0126
42	-0.0030	0.0318	SALR7832	24	0.0000	0.0052
32	0.0129	0.0264	GRAS7845	32	0.0000	0.0120
11	-0.0032	0.0082	SWIS7810	11	0.0000	0.0186

E2 No Bias vs. ALL Adj. Bias

#Obs.	Mean	RMS	Site	# Obs.	Mean	RMS
30	0.0000	0.0150	WLRS8834	30	0.0000	0.0188
130	0.0045	0.0224	MOBL7090	130	0.0000	0.0187
23	0.0010	0.0061	CHAL7237	23	-0.0001	0.0059
94	0.0000	0.0157	MTLR7501	94	0.0000	0.0142
61	0.0050	0.0165	GRAZ7839	61	0.0000	0.0165
22	0.0043	0.0045	POT27841	22	0.0000	0.0007
60	0.0225	0.0307	HALE7210	60	0.0000	0.0189
141	-0.0078	0.0176	MOBL7110	141	0.0000	0.0159
21	-0.0158	0.0314	SWI.7810	21	0.0000	0.0225
28	-0.0117	0.0232	RGO_7840	28	0.0000	0.0178
18	0.0245	0.0346	MLRS7080	18	0.0000	0.0252
48	0.0000	0.0319	SALR7832	43	-0.0004	0.0071
3	0.0000	0.0000	KOM.1868	3	0.0000	0.0000
38	0.0075	0.0330	GRAS7845	38	0.0000	0.0296
12	0.0000	0.0000	MDN21864	12	0.0000	0.0000

ETALON 1 Estimated Biases

Units: mm

70802416	14.61	±4.81
70900512	28.87	±1.62
71100416	-10.61	±5.96
72102312	25.54	±3.51
75010600	58.72	±2.60
78106800	-38.44	±12.81
78325504	37.42	±10.49
78457800	14.26	±3.35
88341000	40.18	±3.11

ETALON 1 Estimated Biases

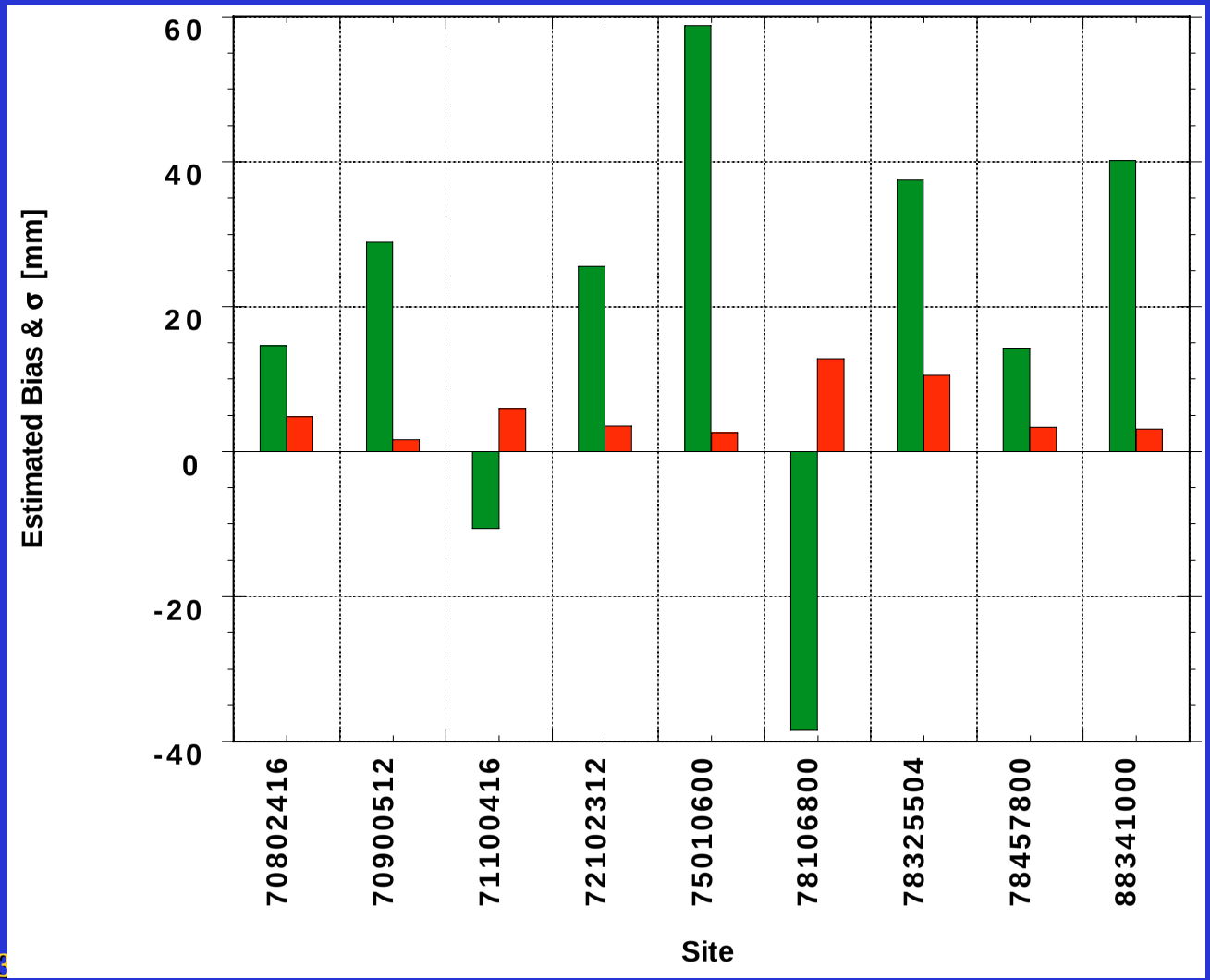

ETALON 2 Estimated Biases

Units: mm

70802419	21.22	±5.19
70900513	21.40	±3.07
71100412	-7.52	±2.36
72102313	28.51	±2.80
75010602	40.85	±3.33
78106801	-25.76	±4.67
78393402	0.03	±3.22
78403501	-19.49	±4.18
78418701	33.94	±39.20
78457801	7.26	±3.54
88341001	39.36	±4.35

ETALON 2 Estimated Biases

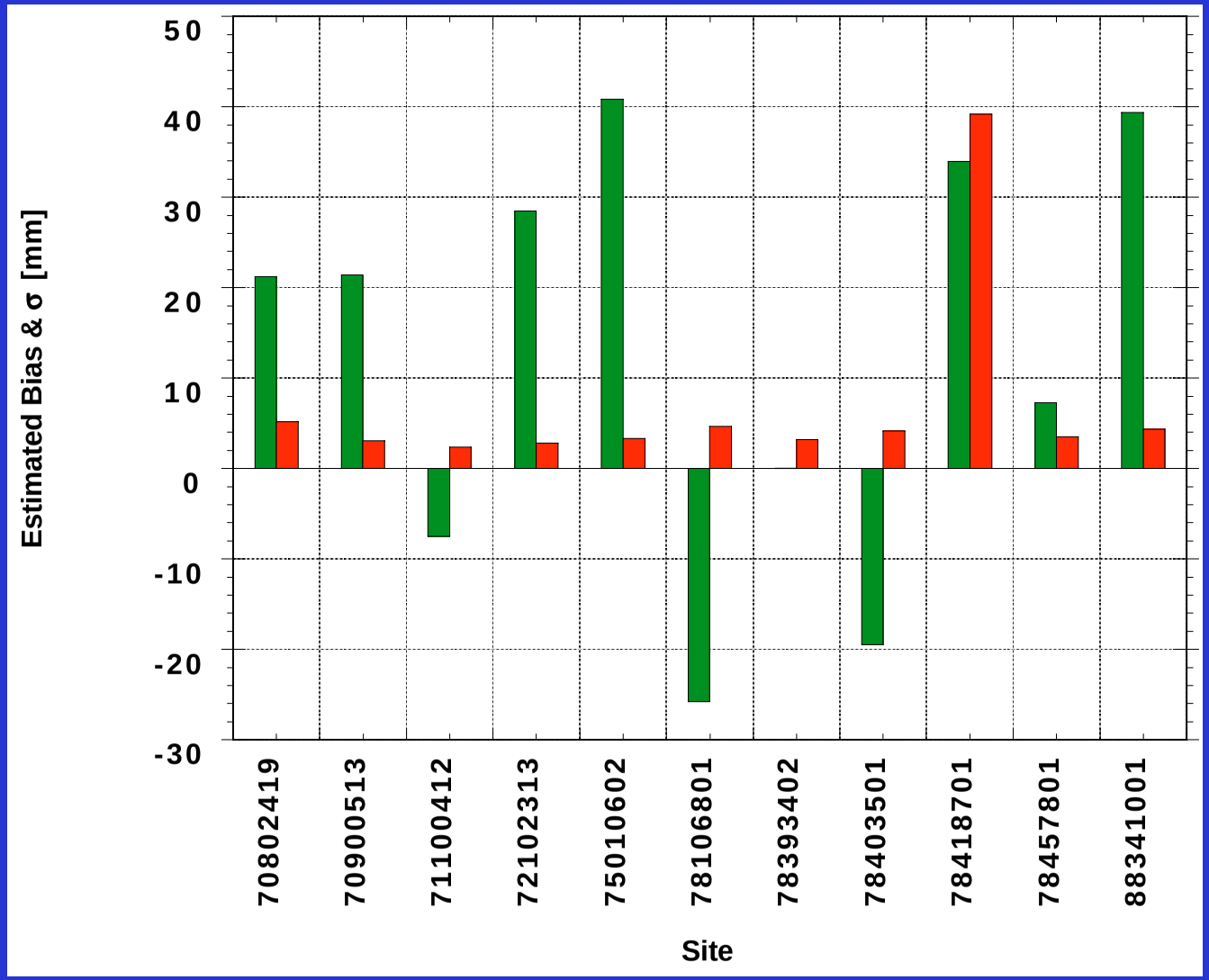

Summary

- Originally adopted CoM offsets (in disagreement with the recently published values), seem to imply that MCP systems (like NASA sites) should apply the revised offsets, closer to the newly published numbers
- Even with these changes taken into account, it seems that there is variation within "types" of receivers, depending on the mode of operation, as it is implied by the different (~ -1 cm) bias for the Monument Peak MOBLAS NASA system
- We need standard assignment of the most appropriate offset value for each site, preferably on a pass-by-pass basis, based on the responsible ILRS WG's results, and the operational regime appropriate for that pass.

Cross section of ILRS satellites

by

David Arnold - 94 Pierce Road, Watertown, MA 02472, 617-924-6812

1. Introduction

The cross section of the satellites tracked by ILRS has been computed using whatever information is available on the design of the arrays and the specifications of the cube corners. The cross section is not constant for any array. It is a function of incidence angle, velocity aberration, wavelength, and polarization if the cube corners are uncoated. The cross section is given by the intensity of the diffraction pattern of the array at the position of the receiver in the far field as determined by the velocity aberration. This report uses diffraction theory to calculate cross section matrices for the arrays at various incidence angles for wavelength 532 nanometers. The velocity aberration limits depend on the altitude of the satellite. The average cross section within the velocity aberration limits is computed at each incidence angle on the array. The average over all incidence angles is also computed and tabulated.

2. Cross section table.

Table 1 lists the current cross section for each satellite on the ILRS webpage and the revised cross section computed using diffraction theory. The minimum and maximum cross section as a function of velocity aberration and incidence angle are also listed for the satellites where there is enough information to do a diffraction calculation.

THEORETICAL CROSS SECTION
(Million sq m)

SATELLITE	ALTITUDE	CURRENT	REVISED		
			Minimum	Average	Maximum
Starlette	950	0.65	1.00	1.80	2.5
Lageos	6000	7.00	9.00	15.00	23.0
Etalon	19000	60.00	-	55.00	-
Topex	1300	2.00	6.00	33.00	83.0
BeaconC	940	3.60	0.00	13.00	35.0
Ajisai	1400	12.00	-	23.00	-
Gfo-1	800	2.00	.07	.50	1.1
Stella	950	0.65	1.00	1.80	2.5
Jason	1300	0.30	.20	.80	1.7
GPS	20000	40.00	-	19.00	-
Champ	500	1.80	.05	1.00	3.4
Westpac	835	0.03	0.00	.04	.4
ERS	800	0.30	.20	.85	1.6
Glonass396	20000	360.00	-	240.00	-
Glonass132	20000		-	80.00	-
Envisat	800	0.30	.20	.85	1.6
LRE	25000	1.25	-	2.00	-
SUNSAT	600	0.20	.04	.40	1.4

Table 1. Current and revised cross section for the ILRS satellites.

3. Diffraction model.

The diffraction calculations have been done using the theory given in SAO Special Report 382, "Method of Calculating Retroreflector Array Transfer Functions", David A. Arnold. The equations model coated or uncoated retroreflectors with a dihedral angle offset. The model does not include any manufacturing imperfections such as roughness or surface curvature. Manufacturing imperfections can result in a loss of cross section in the actual cube corners. These losses are probably a factor of 2 or more. Therefor the theoretical calculations should be considered as an upper limit to the actual cross section. There is no data on the actual "in-orbit' cross section in absolute units although relative measurements between some satellites have been done.

The cube corners on the Japanese satellites are in the shape of a triangle with the corners cut off. There is no model for the reflectivity of this design of cube corner. The Russian satellites are not manufactured to a particular specification. Therefor it is not possible to do an accurate theoretical calculation of the cross section. For satellites where no information is available on the dihedral angle offset, an angle optimized for the particular velocity aberration has been used. If the actual dihedral angle is not optimized, the cross section will probably be lower.

The Japanese satellites are spherical and use uncoated cube corners. Since the LAGEOS satellite is also spherical and uses uncoated cube corners, the cross section of the Japanese satellites is estimated by scaling the cross section of LAGEOS by the reflecting area.

4. Sample diffraction patterns.

Diffraction patterns of various satellites are shown in the report "Retroreflector Array Transfer Functions" available on the web at http://nercslr.nmt.ac.uk/sig/signature.html in PDF and WORD format (Reference 1). Some sample diffraction patterns for LAGEOS from that report are shown in Figure 1 for linear and circular polarization.

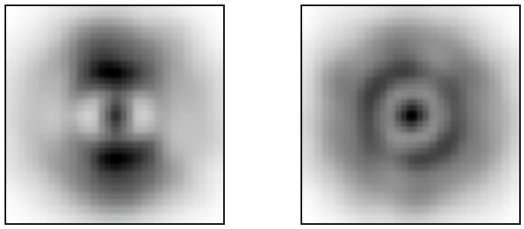

Figure 1. Cross section of LAGEOS for linear polarization (left) and circular polarization (right) at one orientation of the satellite. The axes are -50 to +50 microradians.

The diffraction pattern for linear polarization has a dumbbell shape with the axis of the dumbbell aligned with the polarization vector of the incident laser beam. The diffraction pattern for circular polarization has a more circular shape. The pattern for circular polarization is not perfectly circular because there are a limited number of cube corners that are active at a particular orientation of the satellite. The intensity of the diffraction pattern at the position of the receiver is the cross section of the satellite.

Figure 2 shows some sample diffraction patterns for TOPEX from Reference 1.

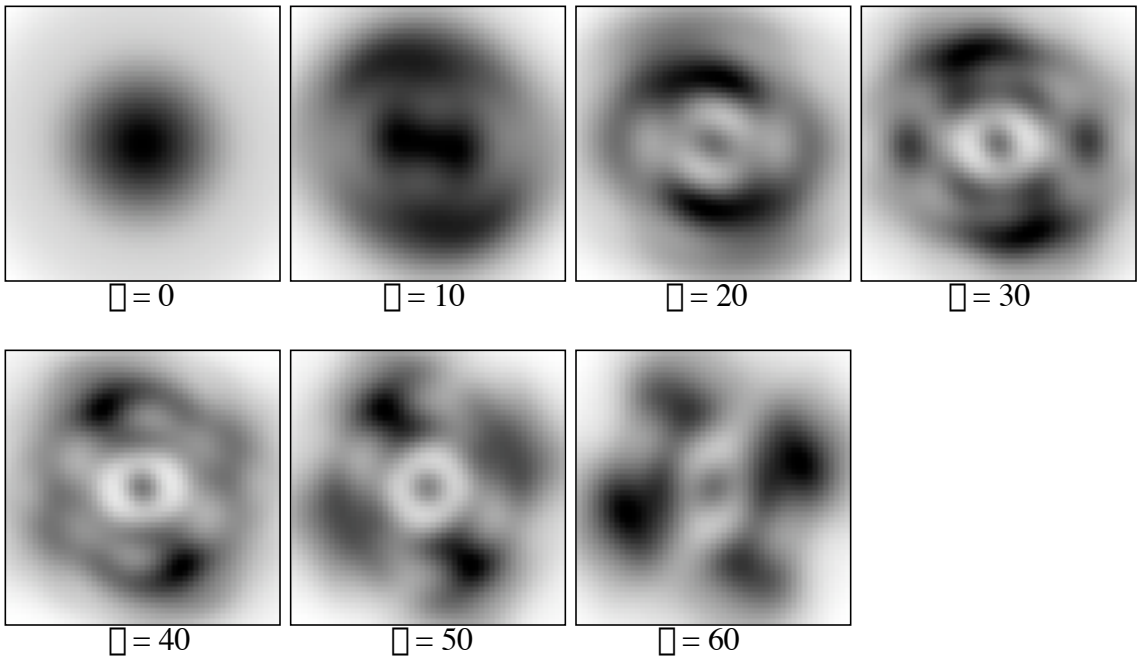

Figure 2. Diffraction patterns of the TOPEX retroreflector array for various incidence angles θ (deg) on the array.

5. Variation of the cross section with incidence angle.

A. TOPEX

As can be seen from figure 2 the cross section varies with incidence angle as well as with the position of the receiver in the far field pattern as determined by the magnitude and direction of the velocity aberration. Table 2 shows a summary of the cross section for TOPEX vs incidence angle on the array.

Cross section of TOPEX (million sq m)

Incidence Angle	Minimum	Average	Maximum	Active area
0	15	20	32	31
10	15	29	40	34
20	16	37	62	37
30	19	44	71	40
40	12	45	83	40
50	12	35	62	32
60	6	22	38	21

Table 2. Cross section statistics for TOPEX. The first column is the incidence angle in degrees, the second the minimum cross section, the third the average cross section between 25 and 50 microradians velocity aberration, the fourth the maximum cross section, and the fifth the total reflecting area in equivalent number of cube corners at normal incidence.

The average of the numbers in the third column is 33 million sq meters. The lowest cross section is 6 million at the bottom of column 2 and the highest cross section is 83 million in column 4 for 40 degrees incidence angle. This is the data that was used to generate the values in Table 1 for TOPEX.

B. SUNSAT

The Sunsat array has a ring of 8 cube corners tilted at 50 degrees with respect to the symmetry axis. There is no pole cube facing the earth such as on the ERS, JASON, GFO, and other similar satellites. The 9 cube arrays on these other satellites form an approximate hemisphere so that the cross section does not vary much with incidence angle. For the Sunsat array, the cross section at normal incidence on the array is very low because all the cube corners are being viewed at a 50 degree incidence angle. This is not far from the cutoff angle of about 57 degrees. The fact that the cross section is very low for normal incidence is not a problem because this only occurs at zenith where the range is shortest. In fact the absence of the pole cube can be an advantage in avoiding a large dynamic range in the signal. However, using a constant cross section in predicting signal strength would result in large errors since there is such a large variation in cross section. Figure 3 shows the variation of the cross section for Sunsat with incidence angle on the array.

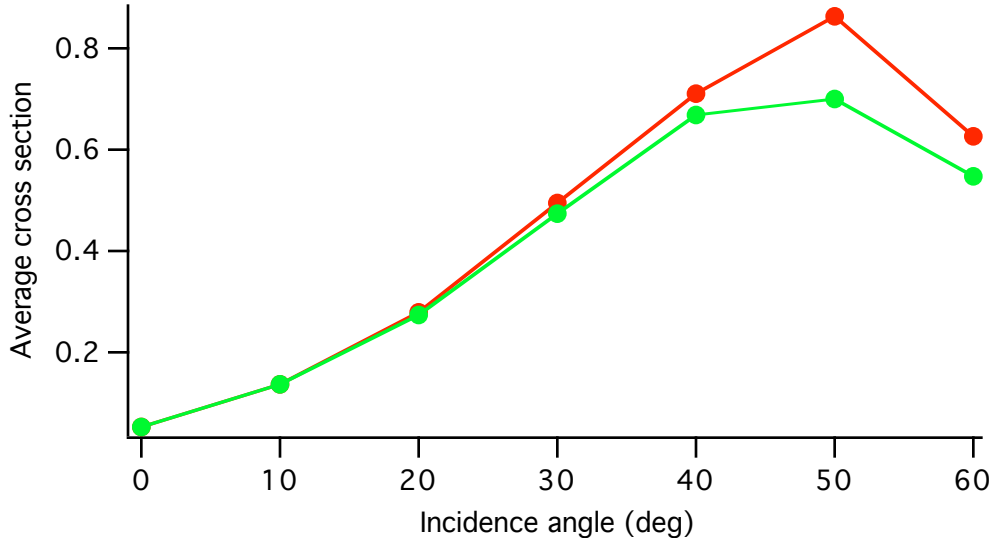

Figure 3. Cross section of Sunsat vs incidence angle (deg) on the array. The top curve (red) is for Theta = 0 deg and the bottom curve (green) is for Theta = 22.5 deg which is between the first two cube corners in the ring.

C. BEACON

Figure 4 shows a diagram of the BeaconC array. There is one panel at the top and 8 panels tilted at a 54 degree angle. The satellite is magnetically stabilized. Figure 5 shows the cross section vs incidence angle on the array. The green curve is between two panels so the cross section is lower. The cutoff angle is about 105 degrees. The cross section is reasonably constant up to about 70 degrees, but using a constant cross section would give a large error near the cutoff angle.

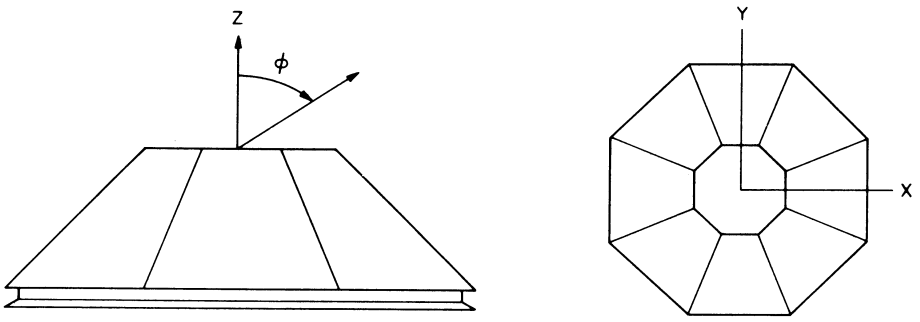

Figure 4. Diagram of the Beacon retroreflector array.

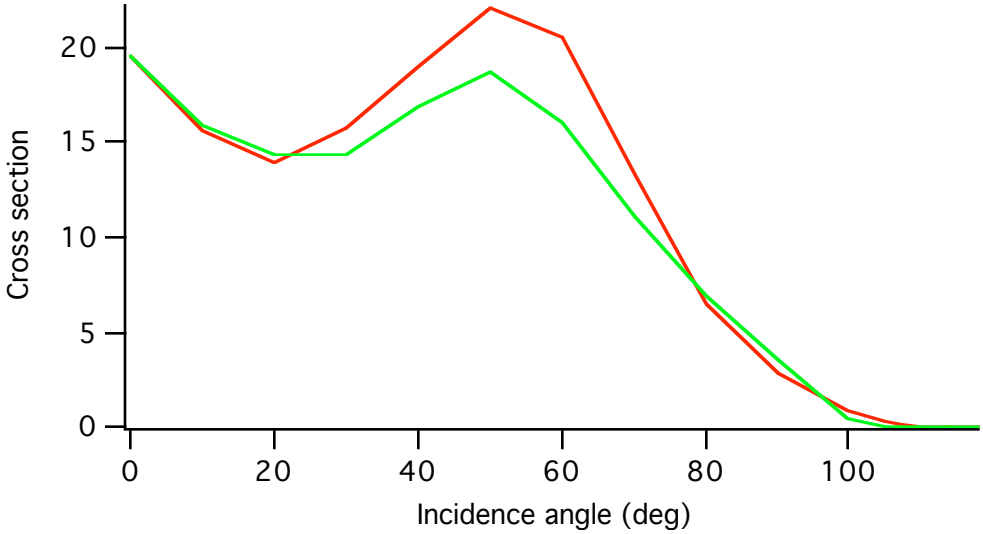

Figure 5. Cross section of the BeaconC array vs incidence angle. The top curve (red) is for Theta = 0 deg and the bottom curve (green) is for Theta = 22.5 deg.

D. CHAMP, GRACE

The cross section of CHAMP is fully documented in References 2 and 3. The array has 4 cubes on a 45 degree pyramid. Table 3 below summarizes the variations with incidence angle on a cube corner using the data in Reference 2. The cross section near zenith (about 40 deg incidence angle on a cube) is fairly low. However, the range is short so the design reduces the dynamic range of the signal strength. Using the cross section vs incidence angle on a cube would help to reduce the error in the predicted signal strength.

Incidence		Flux			Cross Sec.	
Angle	Minimum	Average	Maximum	Minimum	Average	Maximum
0	.0281	.0281	.0281	3.03	3.03	3.03
10	.0172	.0217	.0312	1.85	2.34	3.37
20	.00623	.0102	.0183	.67	1.10	1.98
30	.00216	.00356	.00680	.23	.38	.73
40	.00044	.00081	.00167	.047	.087	.180

Table 3. Cross section of CHAMP, and GRACE vs incidence angle on a cube corner. The cross section in million sq m is the flux times 108.

D. WESTPAC.

The WESTPAC array is designed so that only one cube corner is active at a time. This is done by recessing the cubes so that the cutoff angle is 13 degrees. This creates dead spaces where there is no signal between the cube corners. Table 4 shows the cross section as a function of incidence angle on a cube corner. The cross section is reasonably constant in the range 0 to 9 degrees and then drops off sharply.

Angle	Average	Max
0	.043	.121
1	.043	.202
2	.045	.284
3	.049	.348
4	.054	.380
5	.060	.373
6	.064	.332
7	.062	.266
8	.054	.188
9	.040	.114
10	.024	.055
11	.010	.018
12	.002	.002
13	.000	.000

Table 4. Average and maximum cross section as a function of incidence angle (deg).

E. Spherical, hemispherical, and planar arrays.

For spherical satellites such as LAGEOS, AJISAI, LRE, and ETALON, STARLETTE, and STELLA the cross section will vary some with velocity aberration but the average cross section is nearly independent of incidence angle.

Arrays that are approximately hemispherical such as ERS, ENVISAT, JASON, and GFO have cross section that do not vary much with incidence angle the same as the spherical satellites.

The high altitude satellites such as GLONASS, GPS have planar arrays. The cross section will vary some with incidence angle but the cross section is reasonably constant.

6. Cross section matrices.

The most accurate method of predicting the signal strength is to use the full cross section matrix to calculate the cross section as a function of the magnitude and direction of the velocity aberration. This procedure was used for the range correction on TOPEX. Because of the large size of the array the variations with velocity aberration were a few centimeters. Since signal strength predictions do not require the same accuracy as range corrections there is probably no need to do this for the cross section.

7. Summary.

The cross section of a retroreflector array may be relatively constant for some satellites and may have large variations for others. The cross section vs incidence angle or the full cross section matrix can be used to obtain more accurate signal strength predictions for satellites where there are large variations in the cross section.

8. References.

1. "Retroreflector array transfer functions", David A. Arnold, Proceedings of the 13th International Workshop on Laser Ranging, October, 2002, Washington, DC. Also available on the web at http://nercslr.nmt.ac.uk/sig/signature.html

2. Calculation of the Far field energy distribution of the CHAMP satellite retroreflector, Final report, prepared by: Jakob Neubert, IOF Jena, 1997, Fraunhofer Institut, Angewandte Optik und Feinmachanic.

3. "Investigation of the Effects of Aberration and Diffraction on the Performance of the Laser Reflector for the CHAMP Satellite", prepared by Reinhart Neubert GeoForschungsZentrum Potsdam, Dev.1: Kinematics and Dynamics of the Earth Telegrafenberg A17, D-14473 Potsdam, Germany
Tel.: (49)-331-288-1153, Fax.: (49)-331-288-1111, e-mail: neub@gfz-potsdam.de

4. Detailed data and reports for each satellite are available from the author, or Jan McGarry (NASA), or the Signal Processing Working Group (Graham Appleby).

Germanium flashes in LAGEOS-2 photometry data

by
David Arnold - 94 Pierce Road, Watertown, MA 02472, 617-924-6812
Graham Appleby, Robert Sherwood

1. Introduction

The rotation rate and spin axis of the LAGEOS-2 satellite have been determined by photometric observation of the solar flashes from the front face of the cube corners as the satellite rotates (Reference 1). However, since the flashes from the optical cubes are all the same, there is no way to determine the phase of the rotation using the flashes from the optical cubes.

There are 4 germanium cubes on LAGEOS-2 in holes 4N1, 4N16, 4S9 and 4S24. There are 31 holes in each row. The spacing between 4N1 and 4N16 is 15 holes. However, the spacing between 4N16 and 4N1, which could be considered to be in hole 4N32 if one were to continue the numbering past 31, is 16 holes. This lack of symmetry could be used to determine which germanium cube is being observed if there were a way to distinguish the germanium flashes from the optical flashes.

The flashes from the optical cubes are due to dielectric reflection from the front face. The reflection coefficient at normal incidence is about 4 percent. The germanium cubes are opaque at optical wavelengths and have a solar reflectivity of about 50 percent. The flashes from the germanium cubes should be much stronger than the flashes from the optical cubes because of the higher reflection coefficient.

2. Plots of photometry data

No evidence of stronger flashes from the germanium cubes has ever been reported in the photometry data. I asked Graham Appleby if it would be possible to look through the Herstmonceux data for the rows where the germanium cubes are located to see if there was any evidence of stronger flashes from the germanium cubes. An initial search did not turn up anything unusual.

The failure to find anything was rather perplexing since it seemed that the flashes should be there. I asked for a sample of the data to see if I could find any explanation for the apparent absence of any strong flashes. Robert Sherwood sent me an sample of data that contained a particularly long series of flashes from row 4S.

Figure 1 shows a plot of the data provided by Robert Sherwood. The strongest line in the data is a star. Stars can be distinguished from the flashes by the fact that they have a longer time duration. The flashes from the optical cubes can be seen throughout the plot. The dots above about 100 counts are from the laser which is firing during the first part of the plot. There does not seem to be anything in the plot to indicate the presence of germanium flashes.

The amplitude of the laser pulses is about 1600 counts which puts them off-scale in the plot which only goes up to 200 counts. The laser flashes are very short and are usually contained within one bin which is 1 millisecond long. Occasionally, the laser flash is split between two bins with any combination adding up to about 1600. For example, a laser pulse might be contained in 2 bins of amplitude 100 and 1500 totaling 1600 counts. This is what accounts for the points above 100 in the plot. The laser pulse rate is 10 pps and the optical flashes are at about 1 second intervals.

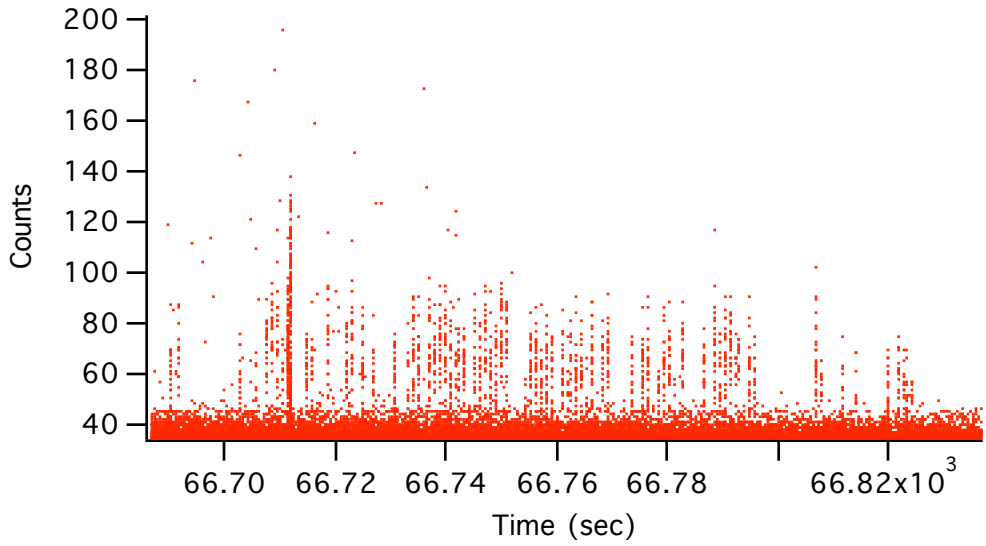

Figure 1. Plot of photometry data from row 4S of LAGEOS-2.

One possibility was that the germanium flashes might be hidden in the noise somehow. Since the laser flashes add noise to the data I decided to first filter out the laser pulses. The optical flashes cover a few tens of bins. This is more frequent than needed to define the shape of the flash. In order to get better signal to noise I averaged sets of 5 data points. With the laser pulses included, it is not possible to plot the data with lines connecting points since this would simply produce a box with amplitude of about 1600. However, lines between points should show the amplitudes more clearly if there were no laser pulses.

After filtering and smoothing the data, I plotted the results with lines connecting points. The results are shown in figure 2. There are 4 strong pulses immediately evident in the plot. The amplitude of the pulses is between about 400 and 550 counts.

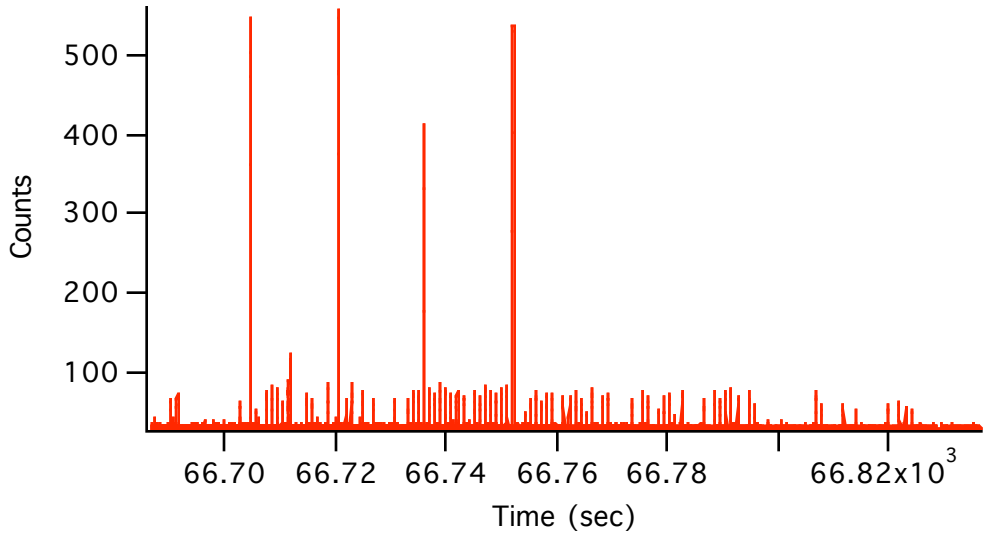

Figure 2. Plot of photometry data with laser pulses removed and sets of 5 points averaged.

Figure 3 shows a plot of the first part of the data with most of the background noise removed and a different filtering and smoothing algorithm. Although there is one optical flash missing, it is evident in the plot that there are 15 optical flashes between the third and fourth germanium flashes. Using the scale determined from this interval, one can determine that there are 14 optical flashes between the second and third germanium flashes and 15 optical flashes between the first and second germanium flashes. This is exactly the spacing one would expect from the positions of the germanium cubes.

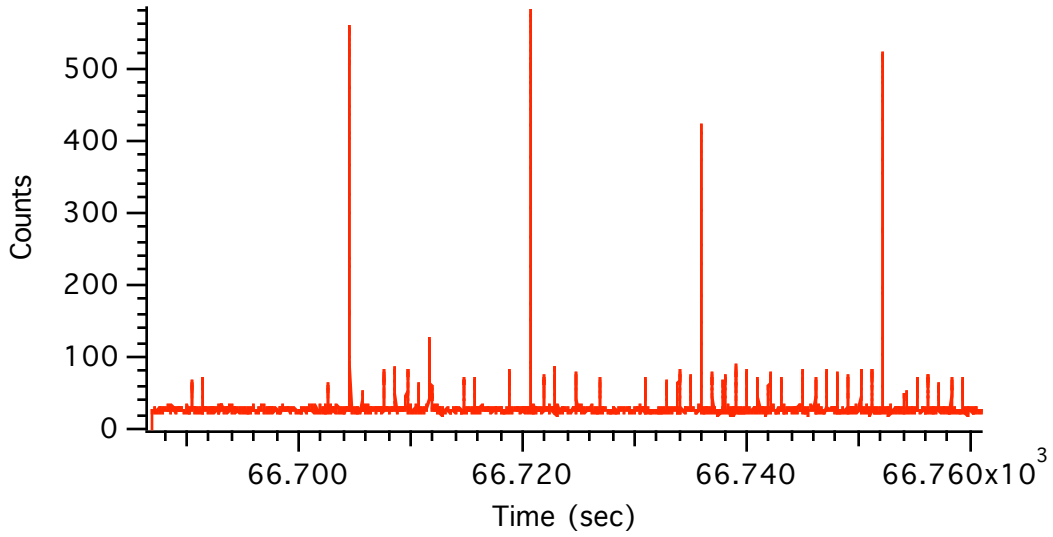

Figure 3. Plot of the first part of the photometry data with most background removed.

3. Interval between flashes.

Table 1 shows a computation of the timing and amplitude of each of the flashes. The columns are the interval between flashes, the average time of the flash, the begin time, end time, width, average amplitude, and peak amplitude. The germanium pulses are clearly evident in the next to the last column. The average amplitude of the germanium flashes ranges from 344 to 464 counts. They are easily distinguished from the optical flashes which range in amplitude from about 52 to 74 counts. The point at 66711 seconds with an amplitude of 78 counts is a star. Its width is .23 seconds which distinguishes it from the optical flashes which have a width of about .025 seconds.

Interval	Time	Begin	End	Width	Average	Peak
3.5736	66690.4136	66690.4036	66690.4236	0.0200	60.5	88.0
0.9971	66691.4086	66691.4007	66691.4165	0.0158	67.8	88.0
11.1499	66702.5586	66702.5506	66702.5666	0.0160	55.9	72.0
2.0279	66704.5925	66704.5785	66704.6065	0.0280	450.8	587.0
3.0320	66707.6226	66707.6105	66707.6346	0.0241	69.8	90.0
1.0091	66708.6310	66708.6196	66708.6425	0.0229	74.0	96.0
1.0179	66709.6480	66709.6375	66709.6585	0.0210	73.5	104.0
1.0100	66710.6530	66710.6475	66710.6586	0.0111	58.7	74.0
0.9301	66711.6956	66711.5776	66711.8135	0.2359	78.8	138.0
3.1240	66714.7141	66714.7016	66714.7265	0.0249	63.3	76.0
1.0220	66715.7326	66715.7236	66715.7415	0.0179	63.4	89.0
3.0319	66718.7665	66718.7555	66718.7775	0.0220	71.3	95.0
2.0121	66720.7811	66720.7676	66720.7945	0.0269	454.0	602.0
1.0340	66721.8141	66721.8016	66721.8266	0.0250	64.1	80.0
0.9950	66722.8086	66722.7966	66722.8206	0.0240	72.2	97.0
2.0339	66724.8430	66724.8305	66724.8555	0.0250	64.5	86.0

2.0391	66726.8771	66726.8696	66726.8846	0.0150	58.8	83.0
4.0449	66730.9260	66730.9145	66730.9375	0.0230	60.3	76.0
2.0201	66732.9390	66732.9346	66732.9435	0.0089	59.4	80.0
1.0120	66733.9596	66733.9466	66733.9726	0.0260	69.0	91.0
1.0060	66734.9651	66734.9526	66734.9776	0.0250	64.9	91.0
1.0339	66735.9930	66735.9865	66735.9996	0.0131	344.5	434.0
1.0061	66737.0056	66736.9926	66737.0186	0.0260	67.9	90.0
1.0039	66738.0075	66737.9965	66738.0185	0.0220	66.9	88.0
1.0160	66739.0235	66739.0125	66739.0346	0.0221	71.2	95.0
1.0061	66740.0311	66740.0186	66740.0436	0.0250	68.9	95.0
1.0170	66741.0481	66741.0356	66741.0605	0.0249	64.0	89.0
1.0040	66742.0531	66742.0396	66742.0666	0.0270	64.9	90.0
1.0229	66743.0750	66743.0625	66743.0876	0.0251	63.1	78.0
2.0270	66745.1006	66745.0895	66745.1116	0.0221	65.4	92.0
1.0160	66746.1150	66746.1055	66746.1246	0.0191	62.1	80.0
1.0141	66747.1321	66747.1196	66747.1446	0.0250	71.0	95.0
1.0130	66748.1436	66748.1326	66748.1546	0.0220	63.2	93.0
1.0119	66749.1535	66749.1445	66749.1625	0.0180	62.3	79.0
1.0090	66750.1665	66750.1535	66750.1796	0.0261	74.7	96.0
1.0211	66751.1851	66751.1746	66751.1956	0.0210	72.9	89.0
0.9950	66752.1815	66752.1696	66752.1935	0.0239	464.9	581.0
2.0380	66754.2105	66754.2076	66754.2135	0.0059	50.6	58.0
1.0107	66755.2288	66755.2183	66755.2394	0.0211	63.7	84.0
1.0142	66756.2445	66756.2325	66756.2565	0.0240	65.5	86.0
1.0271	66757.2671	66757.2596	66757.2746	0.0150	59.8	88.0
1.0057	66758.2774	66758.2653	66758.2895	0.0242	62.3	83.0
1.0150	66759.2894	66759.2803	66759.2984	0.0181	61.3	75.0
2.0061	66761.2980	66761.2864	66761.3095	0.0231	61.0	85.0
1.0291	66762.3264	66762.3155	66762.3374	0.0219	61.2	81.0
1.0160	66763.3440	66763.3315	66763.3565	0.0250	61.8	91.0
0.9969	66764.3395	66764.3284	66764.3506	0.0222	61.1	81.0
2.0252	66766.3671	66766.3536	66766.3805	0.0269	66.8	89.0
2.0438	66768.4064	66768.3974	66768.4154	0.0180	64.8	81.0
1.0011	66769.4095	66769.3985	66769.4205	0.0220	69.7	92.0
4.0489	66773.4554	66773.4474	66773.4634	0.0160	58.4	75.0
2.0260	66775.4855	66775.4734	66775.4975	0.0241	62.8	86.0
1.0150	66776.5014	66776.4884	66776.5144	0.0260	61.7	91.0
2.0440	66778.5354	66778.5324	66778.5385	0.0061	52.7	56.0
1.0000	66779.5425	66779.5324	66779.5525	0.0201	66.0	87.0
1.0080	66780.5524	66780.5404	66780.5644	0.0240	64.2	89.0
2.0320	66782.5850	66782.5724	66782.5975	0.0251	65.7	89.0
4.0441	66786.6260	66786.6165	66786.6355	0.0190	59.6	78.0
2.0369	66788.6659	66788.6534	66788.6784	0.0250	71.2	117.0
1.0172	66789.6790	66789.6706	66789.6874	0.0168	62.2	76.0
1.0060	66790.6895	66790.6766	66790.7024	0.0258	65.7	91.0
1.0078	66791.6958	66791.6844	66791.7073	0.0229	71.0	91.0
1.0022	66792.6996	66792.6866	66792.7126	0.0260	63.7	76.0
2.0468	66794.7438	66794.7334	66794.7543	0.0209	62.6	91.0
1.0021	66795.7416	66795.7355	66795.7476	0.0121	59.8	75.0
11.1410	66806.8875	66806.8765	66806.8984	0.0219	68.8	102.0
1.0199	66807.9024	66807.8964	66807.9085	0.0121	54.8	65.0
4.0591	66811.9590	66811.9555	66811.9624	0.0069	58.9	75.0
2.0310	66813.9890	66813.9865	66813.9915	0.0050	52.5	69.0
6.0760	66820.0690	66820.0625	66820.0755	0.0130	56.8	70.0
2.0199	66822.0920	66822.0824	66822.1015	0.0191	59.2	75.0
1.0039	66823.0984	66823.0863	66823.1104	0.0241	55.7	70.0

Table 1. Computation of the timing and amplitude of the flashes.

4. The amplitude problem

The germanium flashes are clearly visible in figures 2 and 3 but not in figure 1. One problem that is immediately obvious is that the amplitude of the germanium flashes is greater than the 200 counts. In figure 1 the plot scale is limited to 200 counts in order to eliminate the laser pulses which have amplitudes around 1600 and show the optical flashes which have an amplitude under 100 counts.

Figure 4 shows the same data as figure 1 plotted at full amplitude. The germanium flashes can be seen fairly easily in this plot. The concentration of points around 1600 is the laser firings. The laser stopped firing before the last germanium flash. The concentration of dots showing the germanium pulses is above the 200 count cutoff in figure 1. This is why they were not evident in the plot.

The third pulse in figure 4 might not be very obvious by itself against the background noise from the laser flashes. Figure 5 shows the same data as figure 4 but with the laser flashes removed. With the laser flashes removed there is no problem identifying the germanium flashes.

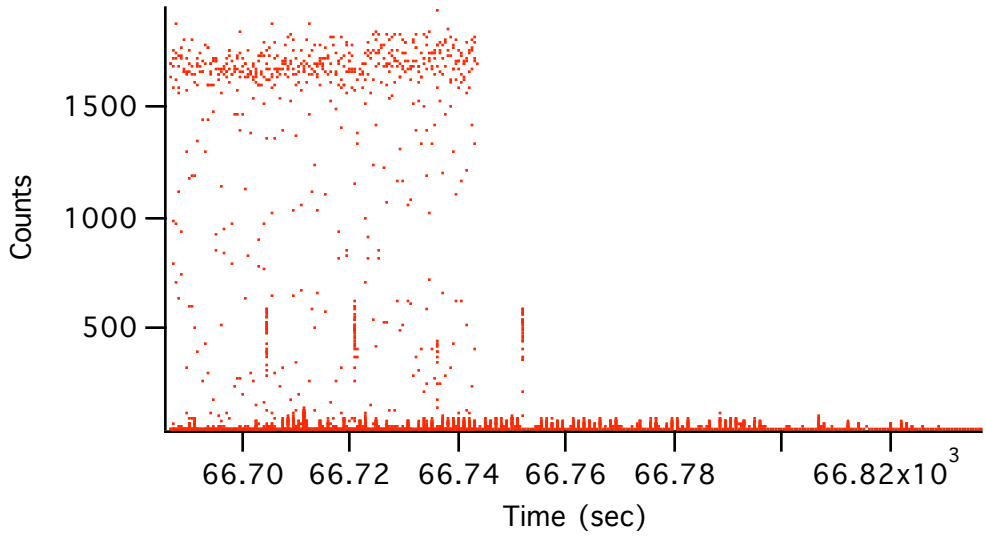

Figure 4. Plot of the complete data set at full amplitude.

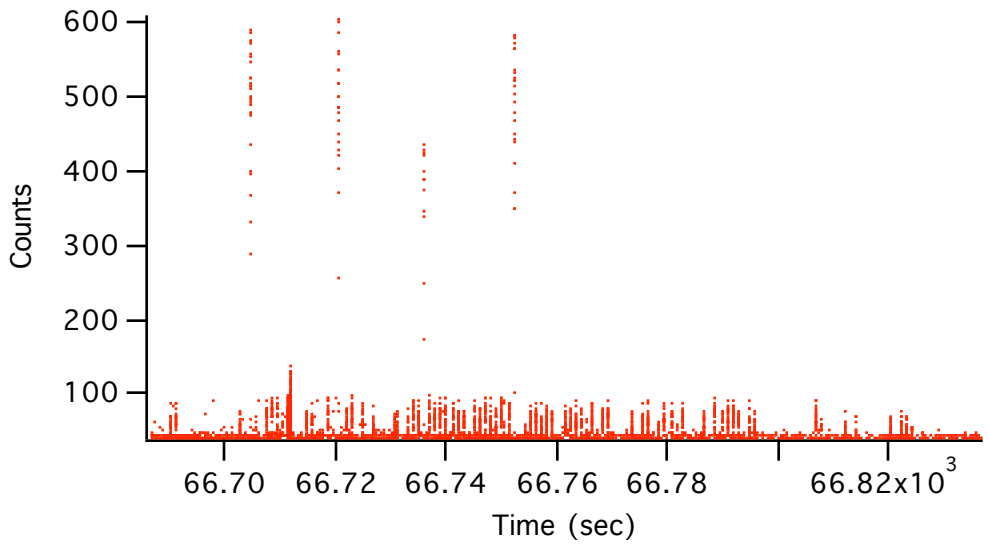

Figure 5. Plot of the data with the laser flashes removed.

5. Fixing the phase

The existence of the germanium flashes makes it possible in principle to determine the phase of the rotation of the satellite in addition to the spin rate and orientation of the spin axis. The extent to which this can be done depends on the density of the data and the stability of the spin rate. At the present time the available data is being cataloged to see what is available. Unfortunately, the spin rate is slowing down. Robert Sherwood has pointed out that as the rate slows there is less likelihood of geting enough data to include at least 2 germanium flashes. It might be possible to use a single flash if it is possible to interpolate the phase angle with sufficient accuracy between data sets having at least two germanium flashes. If there is a germanium flash missing the interval is always the same so that it is not possible to positively identify which cube is being observed.

The germanium cubes could be used in another way to determine the orientation of LAGEOS. The range to a germanium cube varies as the satellite spins. The amplitude of the variation depends on the angle between the line of sight and the spin axis. Range measurements to LAGEOS with a 10.6 micron laser would see only the germanium cubes. Such data could be used to determine the orientation of the satellite. This technique could be used for much slower rotation rates since the 4 germanium cubes with their high index of refraction provide coverage over all satellite orientations.

6. The range correction.

The accuracy goal for LAGEOS was 5 millimeters. The range correction fluctuates over a range of about +/- 5 millimeters as the satellite rotates. The rms error is on the order of 3 millimeters. The main factor limiting the accuracy of the range corrections for LAGEOS is that the orientation is unknown. If the orientation of the satellite were known, the range correction could be computed for that particular orientation. This would result in a significant increase in accuracy to perhaps 1 millimeter. The range correction is a function of polarization for LAGEOS because the cube corners are uncoated. In order to compute the range correction as a function of orientation and velocity aberration it would be necessary to know the polarization (linear or circular) and the angle of the polarization vector if linear polarization is used.

Spectral analysis of the range residuals for LAGEOS using data from the MLRO shows discrete spectral lines that are integral multiples of the rotation rate (Reference 2). This fact could be used as a test of whether range corrections computed as a function of orientation are being correctly applied. The spectral lines should disappear or be significantly reduced in amplitude after the corrections are applied.

7. Summary.

Photometry of sunlight reflected from the cube corners has been routinely used to determine the spin rate and orientation of LAGEOS-2 (Reference 1). Since the reflections from the optical cubes are all the same amplitude, they cannot be used to determine the phase of the rotation. Since the solar reflectivity of the germanium cubes is much greater then the reflectivity of the optical cubes, the phase angle can be determined whenever the viewing angle is such that reflections can be obtained from the rows containing the germanium cubes. Range data from the germanium cubes using a 10.6 micron laser might also be able to determine the complete orientation of LAGEOS. Knowing the complete orientation of LAGEOS would make it possible to apply a range correction as a function of the orientation in order to remove the variations in the range correction as the satellite spins.

8. References.

1. “LAGEOS-2 spin rate and orientation”, Robert Sherwood, Roger Wood, Toshimichi Otsubo, 13th International Workshop on Laser Ranging, October 7-11, 2002, Washington, DC.

2. “Measurement of LAGEOS-2 Rotation by SLR Observations”, G. Bianco, M. Chersich, R. Devoti, B. Luceri, M. Selden, Proceedings of the 12th International Workshop on Laser Ranging, Matera, Italy, 13-17 November, 2000.

Spectral Analysis of LAGEOS Range Data

by
David Arnold - 94 Pierce Road, Watertown, MA 02472, 617-924-6812
Giuseppe Bianco - Agenzia Spaziale Italiana, CGS - Matera

1. Introduction.

The paper "Measurement of LAGEOS-2 Rotation by SLR Observations", G. Bianco, et al. presented at the 12th International Workshop on Laser Ranging (Reference 1) shows that the range residuals from LAGEOS-2 contain discrete spectral lines which are integral multiples of the rotational rate. The lowest frequency is the spin rate. In this paper we show that simulated data for LAGEOS-2 contain the same spectral lines as the range data.

2. Simulation of the rotation of LAGEOS.

The paper "Retroreflector Array Transfer Functions", D. A. Arnold, presented at the 13th International Workshop on Laser Ranging (Reference 2, Figure 6) shows a simulation of the range correction as the LAGEOS satellite spins. The simulations were done using the method described in SAO Special Report 382, D. A. Arnold (Reference 3). Using the data from the simulation V. Luceri and R. Devoti have shown that the simulated data also contains spectral lines that are integral multiples of the spin rate as seen in Figure 1 below.

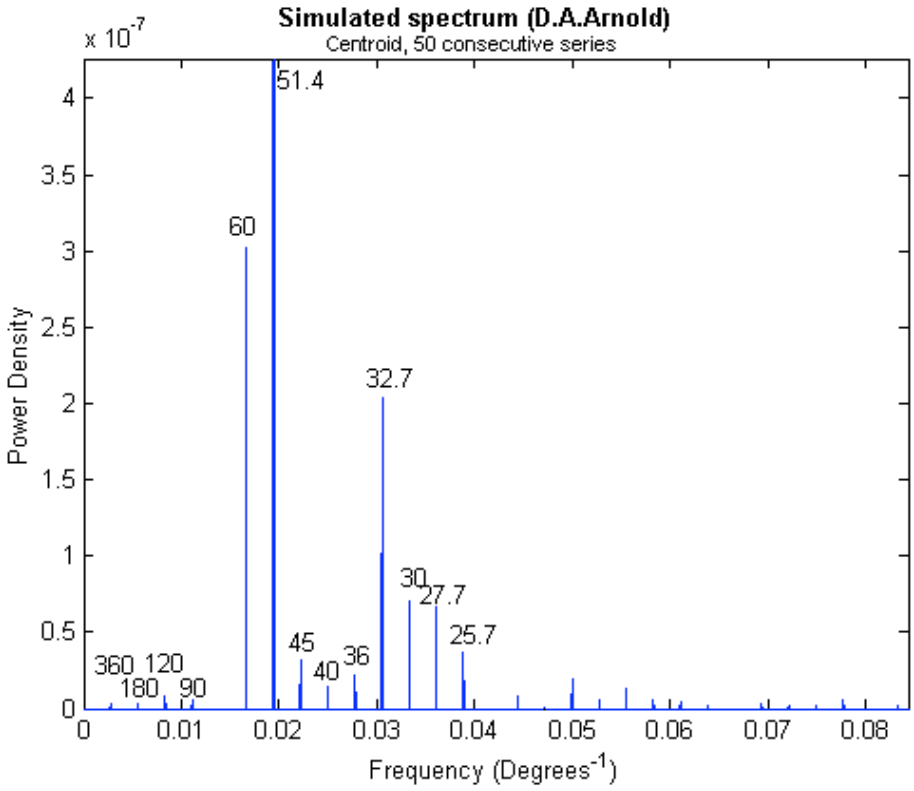

Fig. 1 Spectrum of simulated range residuals of 50 complete LAGEOS-2 rotations as viewed from the satellite's equatorial plane. The periods of the peaks are indicated in units of degrees.

3. Spectral analysis of actual ranging data.

Figure 2 shows a spectral analysis by V. Luceri and R. Devoti of range data from a pass on Oct. 15, 1998. The spectral lines are integral multiples of the rotation rate.

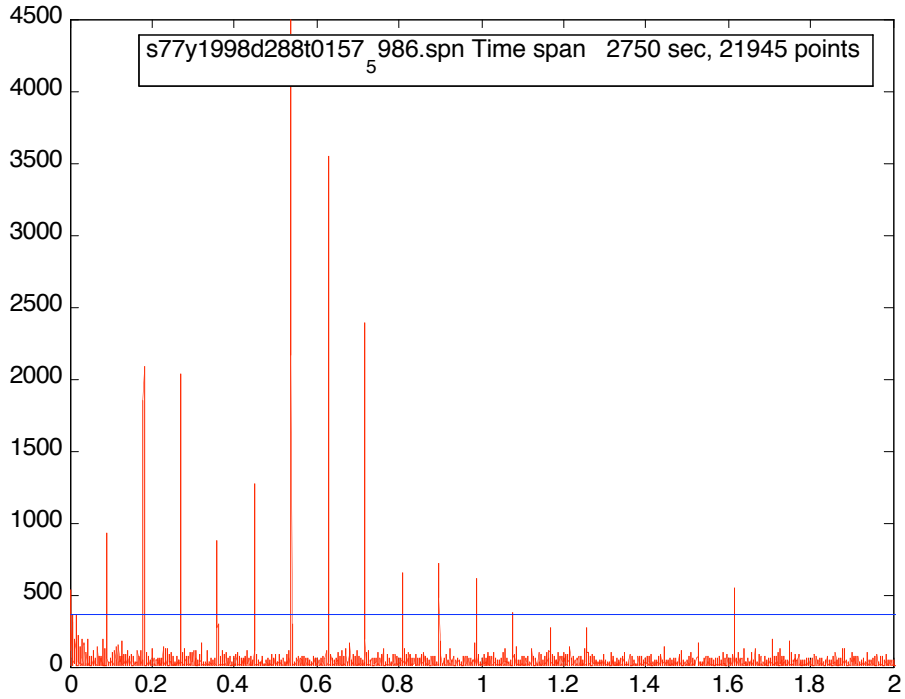

Fig. 2. Spectrum of observed range residuals (MLRO) from a real pass (Oct. 15, 1998), the fundamental period (first peak) is 10.9 sec, all the other peaks are exact harmonics of the fundamental frequency.

Figure 3 shows a second example of spectral analysis of real range data. This pass is from March 21, 2002. The amplitudes of the spectral lines are different but the spectral lines integral multiples of the spin rate. The period of the spin in Figure 2 is 10.9 seconds. In Figure 3 the period has increased to 55.4 seconds.

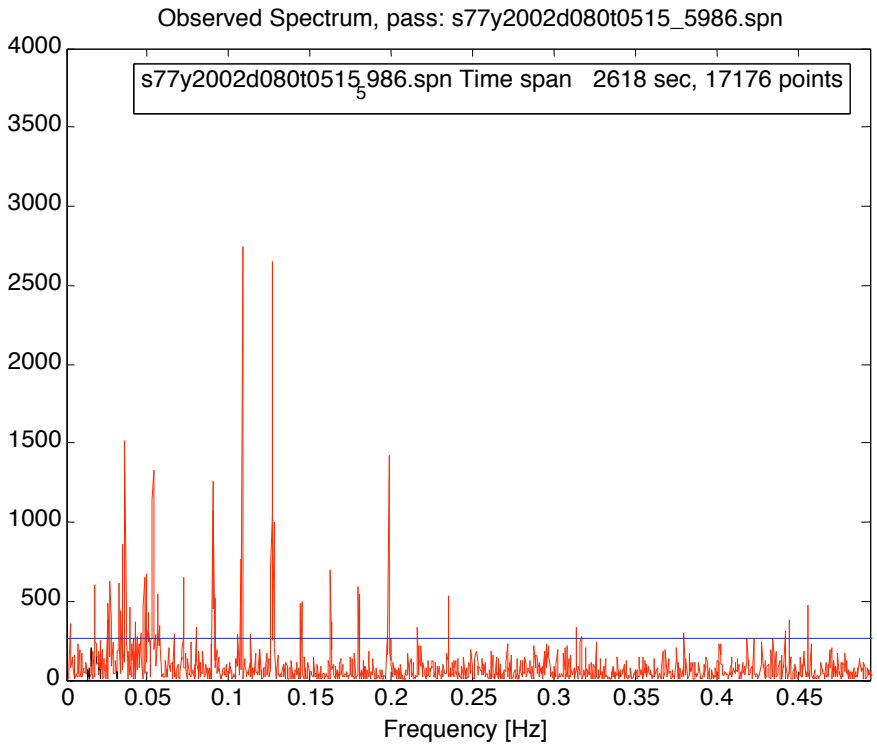

Fig. 3. Spectrum of observed range residuals (MLRO) from a real pass (March 21, 2002), the fundamental period (first peak) is 55.4 sec, all the other peaks are exact harmonics of the fundamental frequency.

4. Comparison of methods of spectral analysis.

The spectral analyses shown in Figures 1, 2, and 3 have been done using the Scargle algorithm for unequally spaced data analysis. The spectral analyses shown in Figures 1 and 3 have been repeated by D.A. Arnold using a different method. In this approach, the equation

$$R = A + B\sin(\omega t) + C\cos(\omega t) \qquad (1)$$

is used to do a least squares fit to the range R as a function of time. For range residuals from an orbital fit, the constant A would be approximately zero. For simulated range corrections, the constant A is about .243 meters. The coefficients B and C can be considered the imaginary and real part of a complex exponential containing the frequency and phase of the spectral component. The spectral analysis is done by varying the frequency ω from the spin rate to the highest spectral frequency. The power P in a spectral component is given by

$$P(\omega) = B^2 + C^2 \qquad (2)$$

Figure 4 shows the spectral analysis of the same data as Figure 1 done by D.A. Arnold using equation (1). The analysis includes only the first 20 spectral lines. Figure 5 shows the same data as Figure 3 analyzed with equation (1). The Scargle method and using equation (1) give essentially identical results.

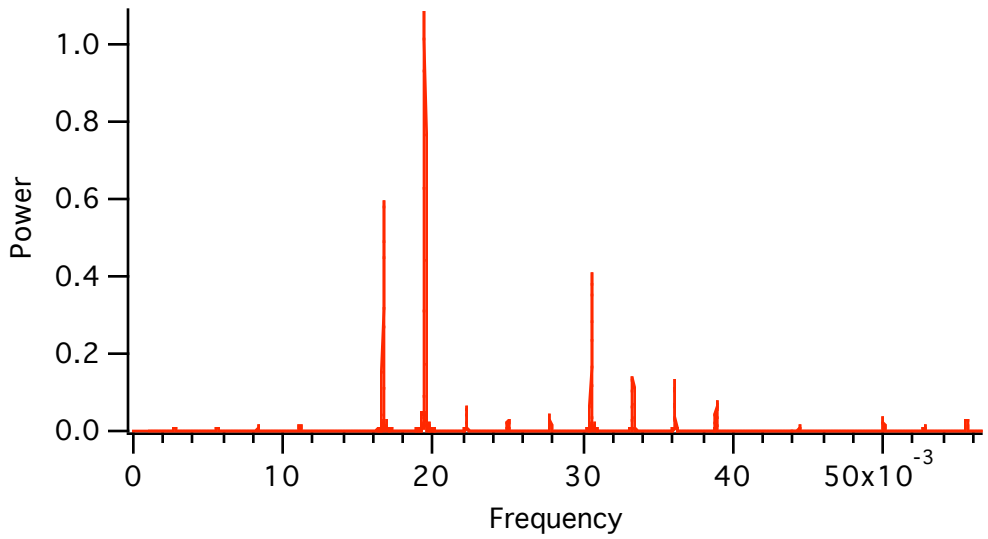

Figure 4. Spectrum of simulated range residuals of 50 complete LAGEOS-2 rotations as viewed from the satellite's equatorial plane. The frequency is in (1/deg).

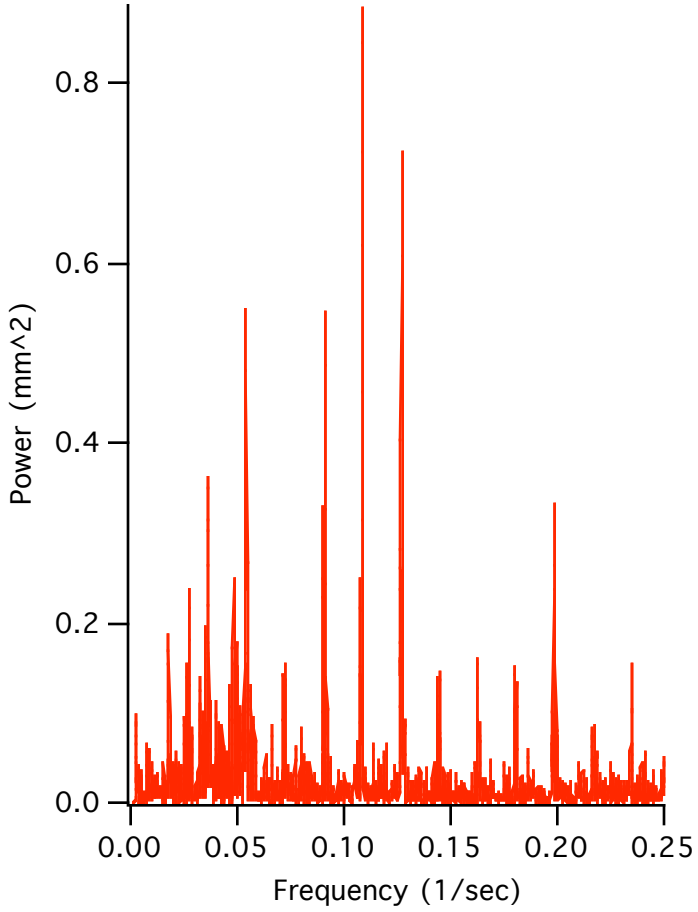

Figure 5. Spectrum of observed range residuals (MLRO) from a real pass (March 21, 2002), the fundamental period (first peak) is 55.4 sec.

5. Dependence on the angle from the spin axis.

In this section simulations are done at various angles from the spin axis of the satellite in order to show the variation in the amplitudes of the spectral lines. The angle between the line of sight and the spin axis is 90 degrees in Figures 1 and 4. In other words, the satellite is being observed from the equator. In Figure 6 the angle with respect to the spin axis is 30 degrees. In Figure 7 the angle is zero (looking directly at the pole).

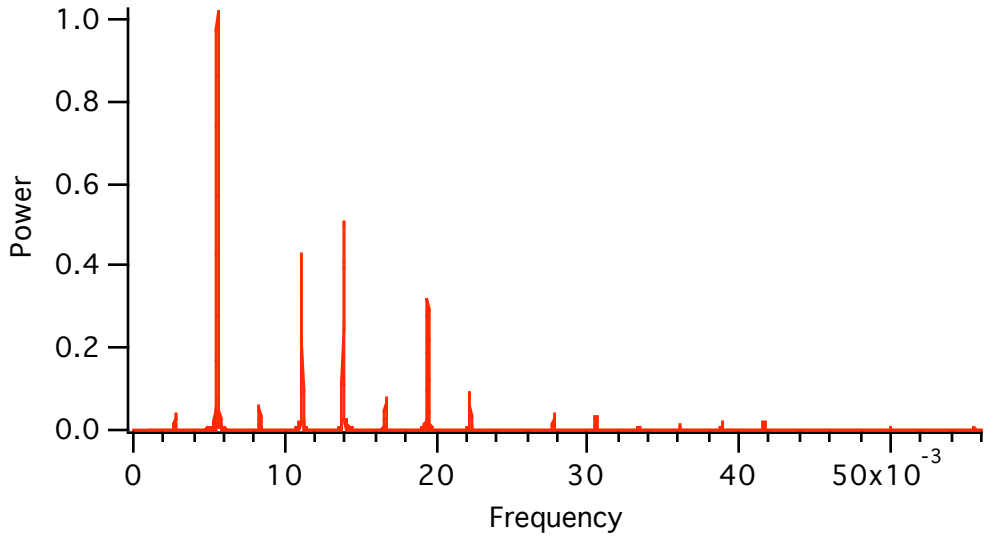

Figure 6. Spectrum with a 30 degree angle between the line of sight and the spin axis.

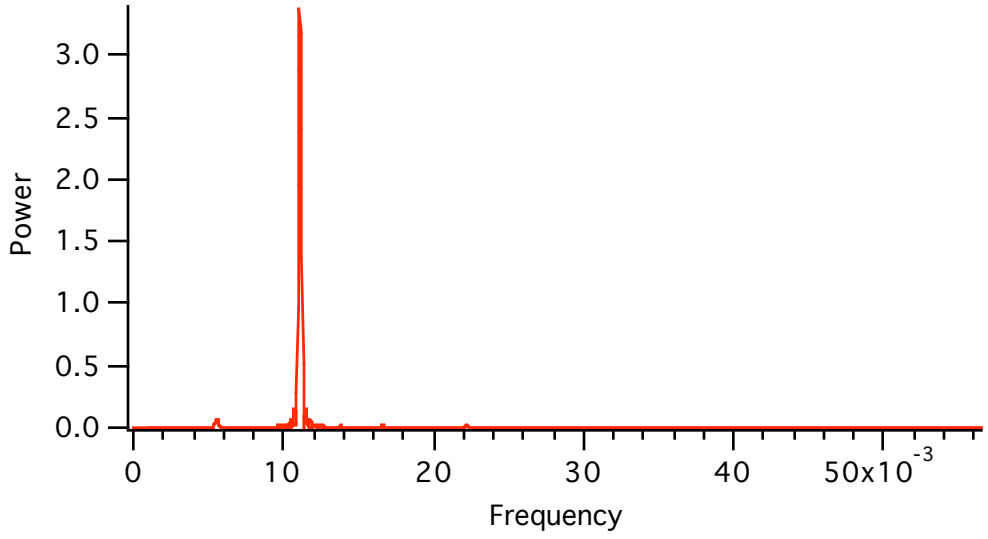

Figure 7. Spectrum looking at the spin axis.

Comparing Figures 4, 6, and 7 we see that the highest frequencies are when the satellite is viewed from the equator. At a 30 degree angle from the pole only the lower frequencies are visible. When looking at the pole there is only one major frequency which is 4 times the spin rate.

6. Phase plot.

Since it has been shown that the spectrum contains only discrete frequencies it is possible to do a spectral analysis with equation (1) using only the known frequencies. In order to obtain accurate results the data must contain an integral number of cycles of each frequency. Figures 8 shows a spectral analysis of the equatorial simulation using only integral multiples of the spin rate with data covering one complete revolution. Figure 9 is a phase plot of the spectral lines in figure 8.

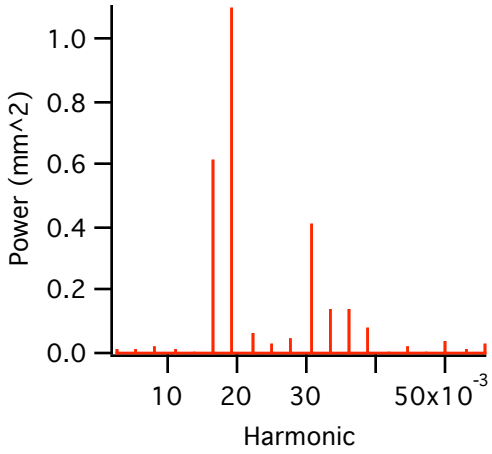

Figure 8. Spectral analysis of one revolution

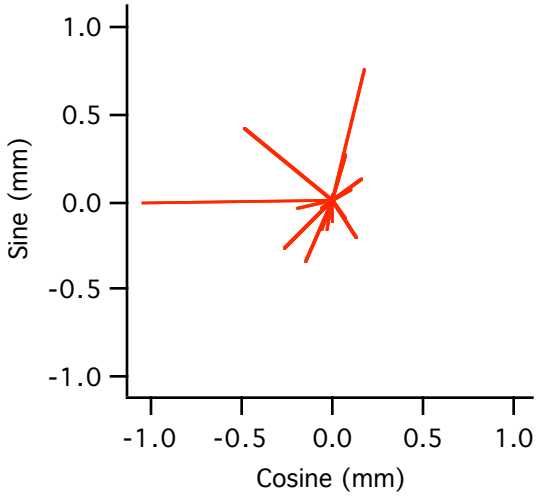

Figure 9. Phase plot of the harmonics

Tables 1 and 2 below shows the data used to plot Figures 8 and 9 respectively.

Period (deg)	Harmonic	Amplitude (mm)	Power (mm^2)	Frequency(1/deg)
360.000	1.000	0.077955	0.006077	0.002778
180.000	2.000	0.072774	0.005296	0.005556
120.000	3.000	0.126817	0.016083	0.008333
90.000	4.000	0.110108	0.012124	0.011111
72.000	5.000	0.032602	0.001063	0.013889
60.000	6.000	0.778751	0.606453	0.016667
51.430	7.000	1.045384	1.092827	0.019444
45.000	8.000	0.251219	0.063111	0.022222
40.000	9.000	0.168907	0.028530	0.025000
36.000	10.000	0.208311	0.043394	0.027778
32.730	10.999	0.638545	0.407740	0.030553
30.000	12.000	0.373327	0.139373	0.033333
27.690	13.001	0.369462	0.136502	0.036114
25.710	14.002	0.270873	0.073372	0.038895
24.000	15.000	0.019269	0.000371	0.041667
22.500	16.000	0.125351	0.015713	0.044444
21.176	17.000	0.025514	0.000651	0.047223
20.000	18.000	0.194486	0.037825	0.050000
18.947	19.000	0.107882	0.011639	0.052779
18.000	20.000	0.166709	0.027792	0.055556

Table 1. Data used to plot Figure 8.

Harmonic	Sine(mm)	Cosine(mm)	Amp(mm)	Power(mm^2)	Phase(deg)
1.0	-0.0017	-0.0779	0.0780	0.0061	181.24
2.0	-0.0363	-0.0631	0.0728	0.0053	209.89
3.0	0.0778	0.1002	0.1268	0.0161	37.82
4.0	-0.0856	0.0693	0.1101	0.0121	309.01
5.0	0.0326	-0.0015	0.0326	0.0011	92.63
6.0	0.7732	0.0932	0.7788	0.6065	83.12
7.0	-0.1402	-1.0359	1.0454	1.0928	187.71
8.0	-0.1900	0.1643	0.2512	0.0631	310.86
9.0	-0.1686	-0.0099	0.1689	0.0285	266.63
10.0	0.1578	0.1360	0.2083	0.0434	49.26
11.0	0.3116	-0.5573	0.6385	0.4077	150.79
12.0	-0.3666	-0.0708	0.3733	0.1394	259.07
13.0	-0.3115	-0.1987	0.3695	0.1365	237.46
14.0	0.2708	0.0075	0.2709	0.0734	88.42
15.0	-0.0191	-0.0023	0.0193	0.0004	263.08
16.0	-0.0808	0.0958	0.1254	0.0157	319.86
17.0	-0.0101	0.0235	0.0255	0.0007	336.80
18.0	-0.1013	-0.1660	0.1945	0.0378	211.40
19.0	-0.1012	0.0372	0.1079	0.0116	290.20
20.0	-0.1666	0.0054	0.1667	0.0278	271.86

Table 2. Data used to plot Figure 9.

7. Reconstructing the function from the spectral lines.

The Fourier coefficients computed for the simulated data can be used to reconstruct the function. The plot below shows the simulated data and the Fourier fit to the data using the spectral lines up to 20 shown in Table 2 above. The fit is not exact. Using a few more terms would probably improve the fit. Some rows of LAGEOS have 32 cubes.

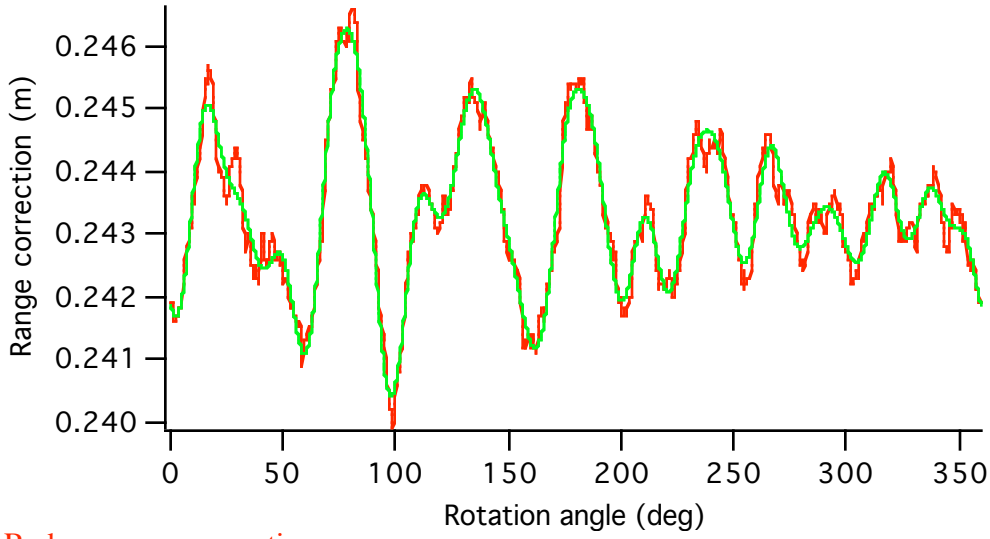

Red = range correction
Green = Fourier fit
Figure 10. Plot of the simulated data and the Fourier fit to the data using terms up to 20.

8. Dependence on the reflecting properties of the cube corners.

A LAGEOS cube corner can lose total internal reflection past about 17 degrees incidence angle depending on the orientation of the cube in its holder. One would expect that the variation of the range correction as the satellite spins would depend on the orientation of each cube in its holder. Figure 11 shows the spectrum looking at the equator with random orientations of the cubes.

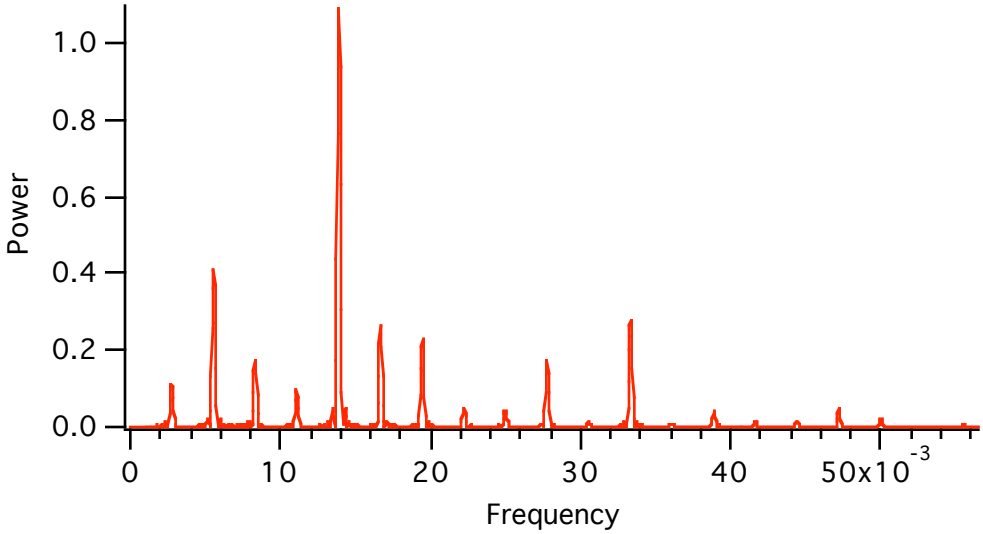

Figure 11. Spectrum looking at the equator with random orientations of the cubes.

Comparing Figure 11 with Figure 4 it is clear that the amplitudes of the spectral lines depend on the orientation of the cubes in their mountings.

9. Methods of computing the spectral lines.

The amplitudes of the spectral lines can be computed in two different ways:

A. If the spectrum of a set of data is unknown, it is necessary to try all frequencies in order to compute the spectral amplitudes. The analysis of the real Lageos data shows a certain amount of noise between the spectral lines. This is to be expected since there are various noise sources present in the data. The analysis of the simulated data shows much less noise between the lines.

B. The terms of a Fourier series are integral multiples of the fundamental frequency and form an orthogonal set of functions over one cycle of the fundamental. There are an integral number of cycles of each frequency in one revolution. Since the Lageos spectrum has been shown to be Fourier series with a finite number of terms it should be possible to solve for the known harmonics from one revolution or an integral number of revolutions by solving only for the known frequencies.

If an interval does not contain an integral number of cycles one will not get the correct amplitudes. Using a long data set with many cycles gives approximately the correct answer even though there may not be an integral number of cycles of each frequency. The error in determining the frequency is inversely proportional to the length of the time interval.

10. Variation of the spectral lines during a pass.

In principle, shorter periods of time could be used in the spectral analysis of real LAGEOS data if the spin rate were known, just as Figure 8 was computed using only one revolution and solving only for the known spectral lines.

Figure 12 below show a spectral analysis done on real data with the pass broken up into eight intervals. We see that the amplitudes of the spectral lines are different in each interval. This is what one would expect if the angle between the line of sight and the spin axis is changing during the pass. The green triangles show the position of the integral spectral lines. The width of the lines is broader and there is more noise between the lines.

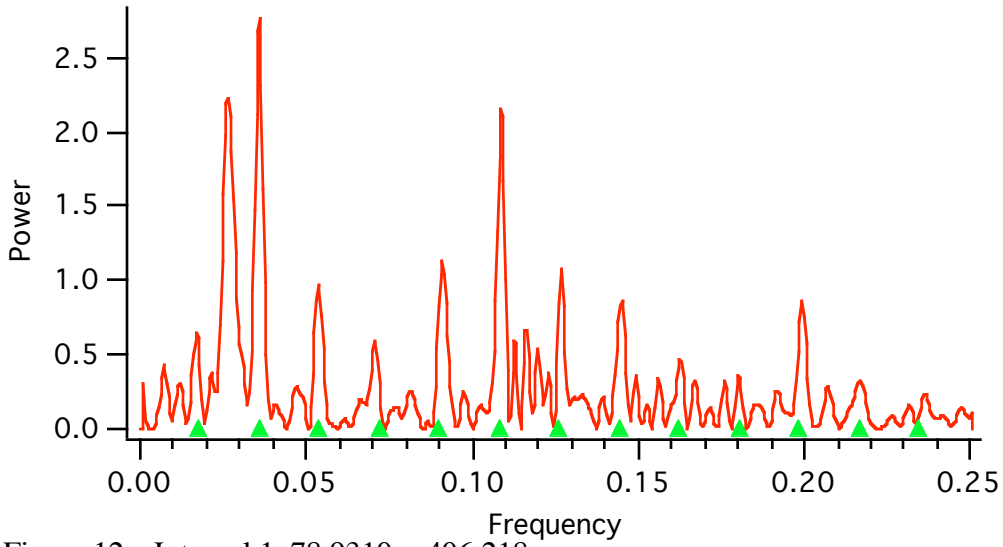

Figure 12a. Interval 1, 78.9310 - 406.218 sec

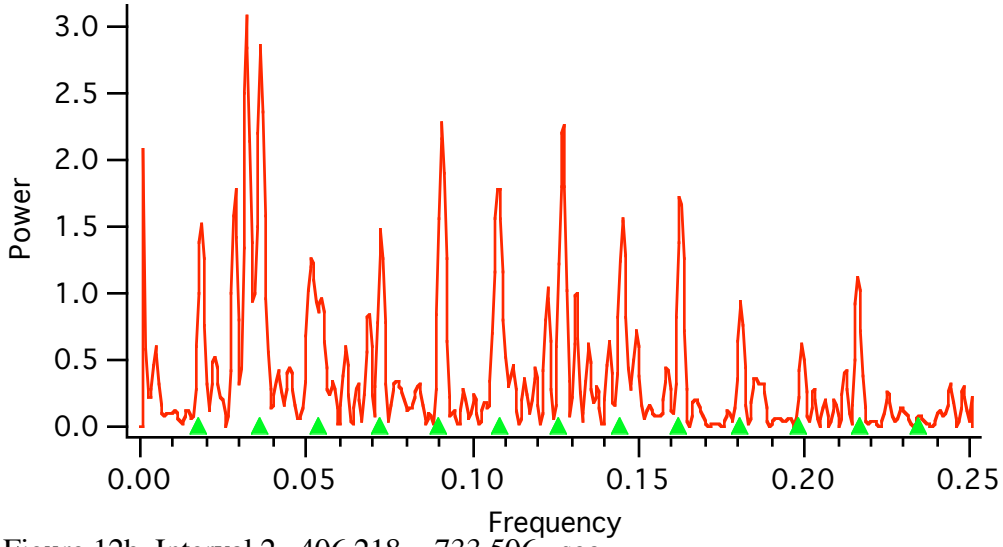

Figure 12b, Interval 2, 406.218 - 733.506 sec

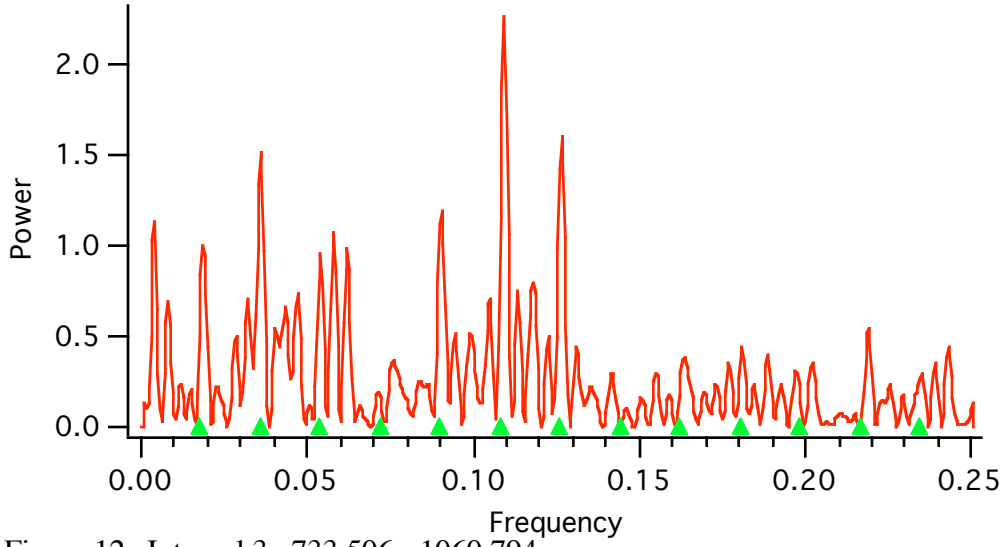

Figure 12c Interval 3, 733.506 - 1060.794 sec

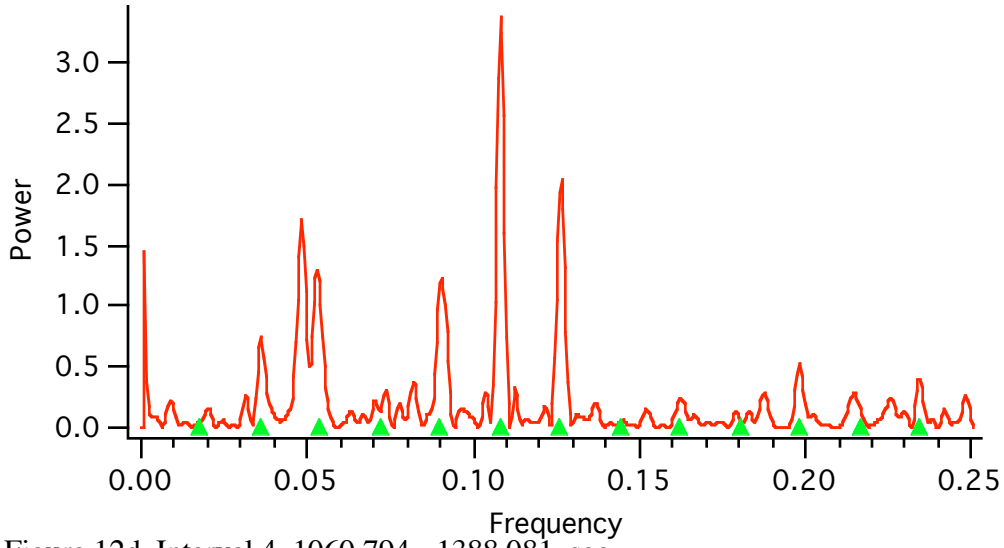

Figure 12d, Interval 4, 1060.794 - 1388.081 sec

The last 4 parts of Figure 12 are shown later in the paper.

11. Experimental verification of the dependence on the orientation of the spin axis.

The simulated data shows that higher frequencies are present when looking at the equator and lower frequencies dominate when looking at the pole. It should be possible to verify this experimentally. The paper "LAGEOS-2 spin rate and orientation", R. Sherwood (Reference 4) shows that the spin rate and orientation of the spin axis can be determined using photometry of the solar flashes from the front face of the cube corners. The spectrum of actual range data could be correlated with the angle between the observing direction and the orientation of the spin axis to see if the frequencies are lower near the pole. Since the angle with respect to the pole is constantly changing during a pass, one should use a short interval consisting of an integral number of revolutions in making the comparison.

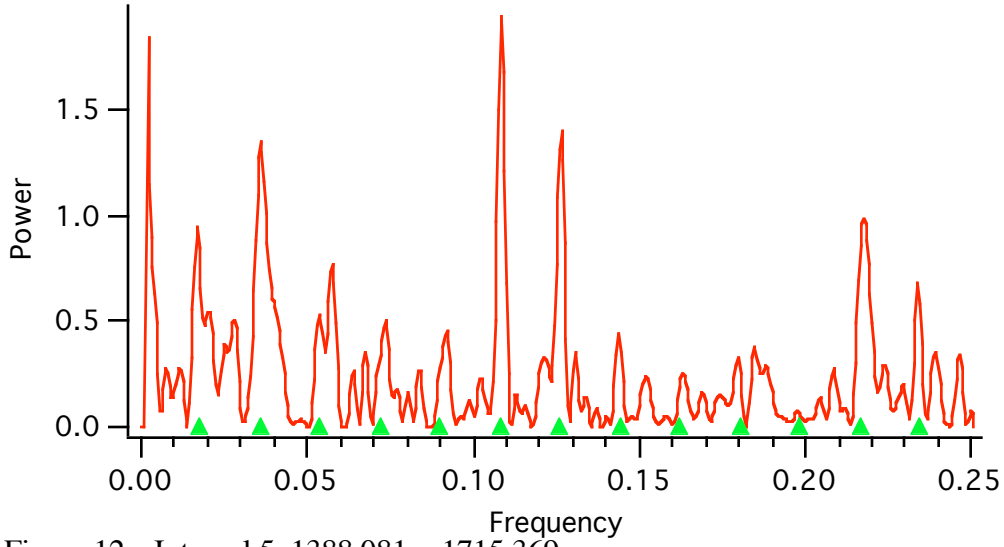

Figure 12e, Interval 5, 1388.081 - 1715.369 sec

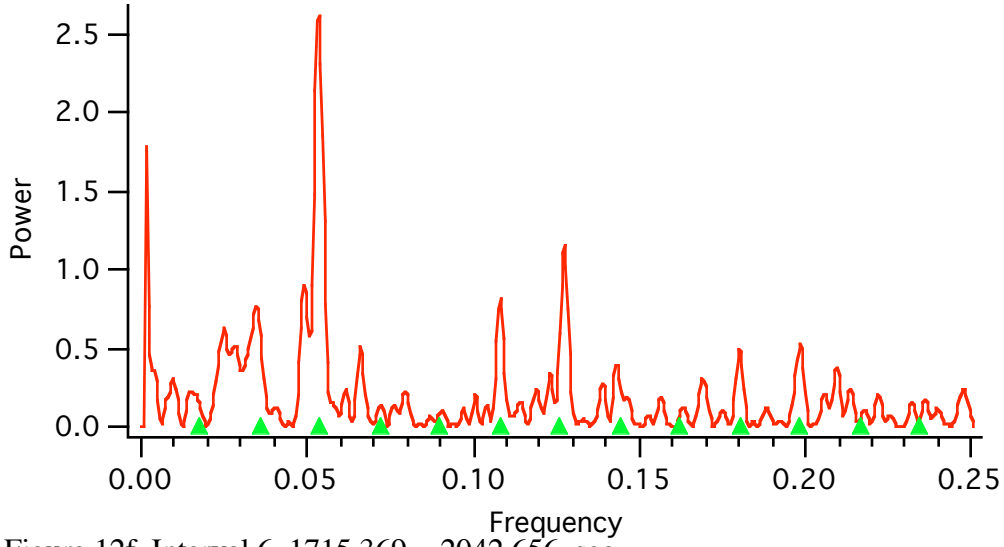

Figure 12f. Interval 6, 1715.369 - 2042.656 sec

12. Determination of the phase of the rotation using the range data.

Since the spin axis and orientation can be determined by photometry (Reference 4), it might be possible to determine the phase of the rotation using the range data. Since the frequencies of the spectral lines are known one could do a spectral analysis of an integral number of rotations. This can be used to reconstruct the range variations as a function of time as was done in Figure 10 of this report. The simulation program can be used to compute the predicted range variations for the time interval using an arbitrary starting phase of the rotation. The two curves could then be compared to try to match up the phase. A second approach suggested by G. Appleby is to vary the phase from 0 to 360 in the simulation and look for the phase angle that minimizes the rms difference between the simulation and the actual data. A third approach would be to add the phase angle to the orbital solution. This would require a starting value of the phase angle since the orbital solution is a non-linear least squares iteration.

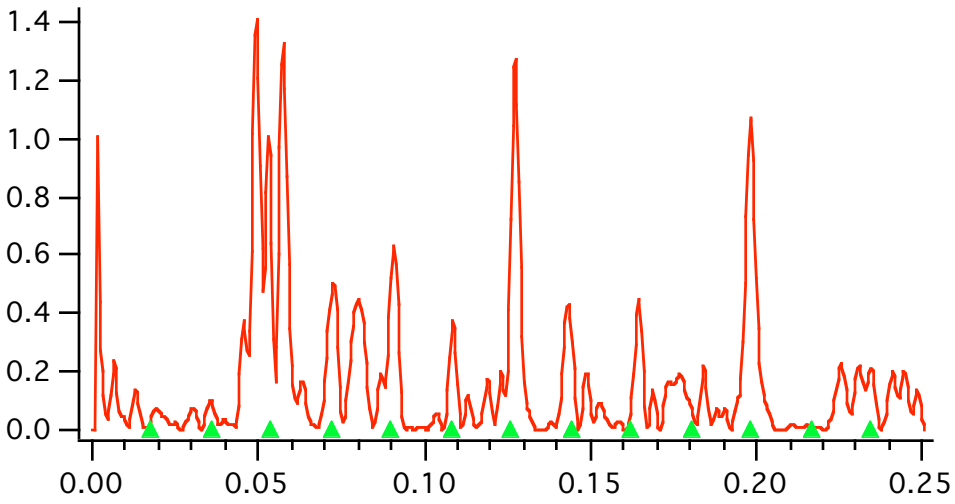

Figure 12g. Interval 7, 2042.656 - 2369.944 sec

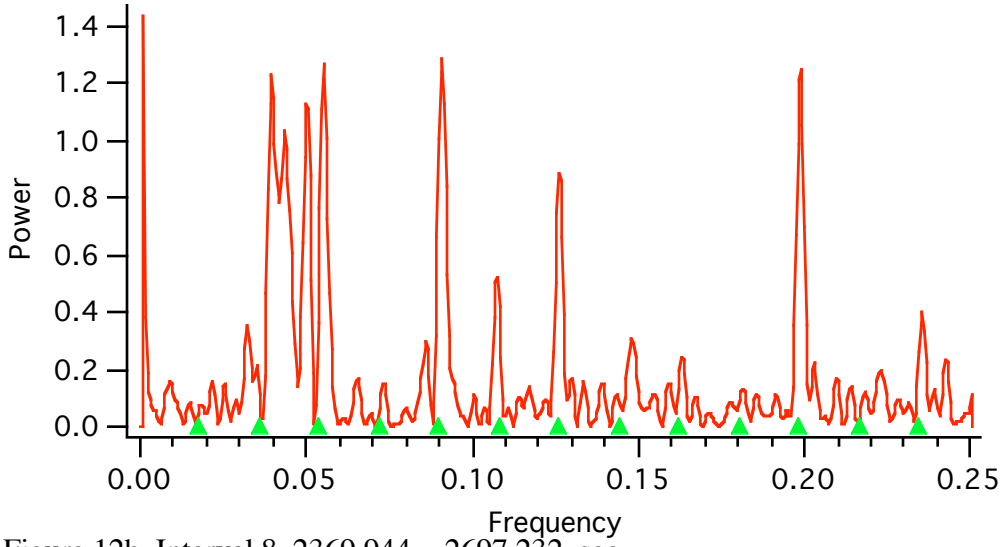

Figure 12h. Interval 8, 2369.944 - 2697.232 sec

13. Other methods of determinating the phase angle.

It has been shown recently that the phase of the rotation of LAGEOS can be determined by observation of the solar flashes from the germanium cubes (see "Germanium flashes in LAGEOS-2 photometry data", David A. Arnold, presented at this workshop). Since the amount of data on the germanium flashes is very limited it may be difficult to use this data to determine the phase throughout the whole period of the photometry. However, it could be used as a starting value for computing the phase in an orbital solution as described in Section 12.

The orientation of LAGEOS could, in principle, be determined by pulsed and CW infrared ranging to the germanium cube corners. This technique is discussed on Pages 187 and 188 of the report "Optical and infrared transfer function of the LAGEOS retroreflector array", D.A. Arnold (Reference 5).

14. Summary and conclusions.

Spectral analysis of simulated and actual LAGEOS range data shows spectral lines that are integral multiples of the spin rate. This seems reasonable since there are an integral number of cube corners in each row on the satellite. The amplitudes of the spectral lines depends on the reflecting properties of the cube corners and the angle of incidence with respect to the spin axis.

15. Acknowledgements

The authors wish to express their appreciation to V. Luceri and R. Devoti for their technical assistance in providing laser range data and doing the analyses shown in the Figures 1, 2, and 3 of this report.

16. References

1. “Measurement of LAGEOS-2 Rotation by SLR Observations”, G. Bianco, M. Chersich, R. Devoti, B. Luceri, M. Selden, Proceedings of the 12th International Workshop on Laser Ranging, Matera, Italy, 13-17 November, 2000.

2. “Retoreflector Array Transfer Functions”, David A. Arnold, Proceedings of the 13th International Workshop on Laser Ranging, Washington, DC, October 7-11, 2002. Also available on the website http://nercslr.nmt.ac.uk/sig/signature.html.

3. “Method of calculating retroreflector-array transfer functions”, David A. Arnold, Smithsonian Astrophysical Observatory SPECIAL REPORT 382.

4. “LAGEOS-2 spin rate and orientation”, Robert Sherwood, Roger Wood, Toshimichi Otsubo, 13th International Workshop on Laser Ranging, October 7-11, 2002, Washington, DC.

5. “Optical and infrared transfer function of the LAGEOS retroreflector array”, Grant NGR 09-015-002, David A. Arnold, May 1978, Smithsonian Astrophysical Observatory.